NTNU
Norwegian University of
Science and Technology

Cation Nonstoichiometry of La_2CoO_4

Nini Karlsen

Chemical Engineering and Biotechnology
Submission date: July 2017
Supervisor: Geir Martin Haarberg, IMA
Co-supervisor: Tetsuya Uda, Kyoto University

Norwegian University of Science and Technology
Department of Materials Science and Engineering

Preface

This master thesis is written as part of the subject TMT4900. This subject is part of the Master program; Chemical Engineering and Biotechnology at the Department of Material Science and Engineering at the Norwegian University of Science and Technology, NTNU. The work was carried out at the Department of Material Science and Engineering at Kyoto University the spring of 2017. Professor Geir Martin Haarberg of NTNU has been my supervisor, and Professor Tetsuya Uda of Kyoto University has been my co-supervisor during this work. The work performed in this thesis was suggested by Emeritus Professor K.T. Jacob at the Indian Institute of Science.

I would like to thank my supervisors Professor Geir Martin Haarberg and Tetsuya Uda for their great support and advice throughout the work of this thesis. Their guidance and opinions have been very helpful, and I highly appreciate the help they have given me. I would also like to thank Professor Geir Martin Haarberg for making my stay in Japan possible and Professor Tetsuya Uda for letting me perform my work at his laboratory at Kyoto University and accepting to be my supervisor. I owe a great thank you to Kyoto International Forum for Environment and Energy (KIFEE) for supporting my stay in Japan by giving me a mobility grant. Also, I would like to thank Assistant Professor Naoyuki Hatada for useful discussions and sharing his knowledge with me. Lastly, I would like to thank master students Katsuhiro Ueno and Katou Kouhei for guiding me through experimental procedures and helping me perform EPMA and XRD measurements. I am very greatful for the generosity and help the students have giving me throughout my stay in Japan.

Abstract

In this thesis, the cation nonstoichiometry and composition range of the La_2CoO_4 phase in the La-Co-O system were investigated and compared to earlier studies. There is a controversy over the cation nonstoichiometry of La_2COO_4, and the La/Co ratio has been reported to be both 1.83 and 2 in different papers. The objective of this work is to clarify the cation nonstoichiometry of La_2CoO_4.

Two samples were prepared with different La:Co ratio, one La-rich and one Co-rich sample. The samples were synthesised using the nitrate freeze-drying method before being heat treated at the temperatures 900°C and 1100°C. In addition, low-temperature oxidation was performed. The La/Co ratios were investigated using XRD, EPMA-WDS and TEM-EDS.

Heat treatment of the La-rich and Co-rich samples at 1100°C resulted in samples containing the La_2CoO_4 phase with the average La/Co ratio of 2.0550 ± 0.0158 and 1.997 ± 0.0056, respectively. This indicated that the cation stoichiometry lies close to the stoichiometric value, but showed evidence that the compound might have a small composition range. The results of low-temperature oxidation of these samples did not show any evidence of any changes which indicated that a La-deficient La_2CoO_4 phase was formed. Changes in lattice parameters were observed, which was consistent with earlier studies indicating that the oxidation leads to oxygen excess in the compound, giving the formula $La_2CoO_{4+\delta}$.

Heat treatment of the samples at 900°C resulted in the same three-phase composition containing La_2CoO_4. The slow reaction rate led to the samples not being fully equilibrated which made it difficult to draw any conclusions on cation nonstoichiometry of La_2CoO_4 from the data collected.

Sammendrag

I dette arbeidet er formålet å undersøkte kationikkestøkiometri og komposisjonsområdet av La_2CoO_4 fasen i La-Co-O systemet, og sammenligne resultatet opp mot tidligere arbeid. Det er uenigheter angående kationstøkiometrien i La_2CoO_4, hvor La/Co forholdet har blitt rapportert til å være både 1.83 og 2 i tidligere studier. To prøver med ulikt La:Co forhold; en La-rik og en Co-rik prøve, var syntetisert gjennom nitratfrysetørkningsmetoden, før de var varmebehandlet ved 900°C og 1100°C. I tillegg var lavtemperatursoksidering utført. Prøvene og La/Co forholdet var analysert og karakterisert ved hjelp av XRD, EPMA-WDS og TEM-EDS.

Varmebehandlingen ved 1100°C resulterte i en La_2CoO_4 fase i både den La-rike og Co-rike prøven med et gjennomsnittlig La/Co forhold henholdsvis lik 2.0550 ± 0.0158 og 1.997 ± 0.0056. Dette resultatet indikerer at kationstøkiometrien i La_2CoO_4 ligger nærme den støkiometriske verdien, og at et lite komposiosjonsområde kan eksistere rundt denne verdien. Fra resultatet av lavtemperatursoksidasjon av disse prøvene var det ikke mulig å se noen indikasjon på at en La_2CoO_4 fase med underskudd av La ble dannet. Forandringer i gitterparamterene ble observert som var i samsvar med tidligere arbeid og indikerer at oksidasjonen førte til overflødig oksygen i fasen utrykt i formelen $La_2CoO_{4+\delta}$.

Varmebehandlingen av prøvene ved 900°C førte til den samme trefase komposisjonen i begge prøvene som inneholdt La_2CoO_4. Reaksjonshastigheten under varmebehandlingen var sakte ved 900°C som førte til at prøvene ikke var nådde likevekt. Dette gjorde det utfordrende å bestemme kationstøkiometrien i La_2CoO_4 ut fra resultatene.

Contents

Chapter 1

Introduction

1.1 Motivation

The physical properties and structural chemistry of perovskite-like oxides have been studied extensively over the past decades, due to their wide range of properties and possible applications. Perovskites and perovskite-like structures show interesting properties such as ferromagnetism, ferroelectricity, piezoelectricity, good conductivity and superconductivity [1]. These oxides have been suggested to be used in several applications such as catalysts in combustion engines and electrodes in batteries and fuel cells. In the latter case, there exist several different types of fuel cells with different designs and advantages. Proton exchange membrane fuel cell (PEMFC), polymer electrolyte fuel cell (PEFC), molten carbonate fuel cell (MCFC), phosphoric acid fuel cell (PAFC), alkaline fuel cell (AFC) and solid oxide fuel cell (SOFC) are some of the types of fuel cells that exist today. Of these, SOFC has been given attention, because of its good properties such as high efficiency, good reliability, and advantages with the flexibility of fuels, and it is close to being marketed as a combined heat and power generation system [2].

However, there is still need for research and improvement of the SOFC design. There has been especially interest in reducing the operating temperature, which causes several problems that increase the operation cost of SOFC [3, 4]. Improvement in the durability, stability, and reliability can also be achieved by reducing the operating temperature, which is necessary for SOFC to be used commercially. An important part of improving the SOFC design is

to have breakthroughs within material selections and concepts. Therefore considering different electrolytes and also the electrode material is an important part of the research and development.

Perovskite and perovskite-like structures are seen as suitable candidates to be used in SOFC, especially as electrode materials [2]. The perovskite-like oxides found in the La-Co-O system are some of the materials that are interesting to study for this purpose. Their properties such as stability, conductivity, and their structural chemistry have therefore been extensively studied. It has been found that several of the oxides found in the La-Co-O system has show significant deviations from stoichiometry. Properties of inorganic compounds are known to be dependent of the nonstoichiometry and defects of the compound, which makes it important to increase the knowledge of this field [5].

Earlier investigations of the ternary oxide La_2CoO_4 have shown that it exhibits large deviations from stoichiometry [6]. There has been some controversy over the true stoichiometry of the La_2CoO_4, and different cation ratios have been reported. J.T Lewandowski *et al.* [7] reported in their paper that the compound had a significant La cation deficiency and proposed the stoichiometry $La_{1.83}CoO_{4-x}$. Others have reported the cation ratio La:Co to be 2:1 and the compound having an excess of oxygen [8]. The work of this master thesis will investigate if the deviations from stoichiometry in the ternary oxide La_2CoO_4 can be explained by cation nonstoichiometry.

1.2 Aim of this study

The first objective of the work of this thesis is to investigate the cation nonstoichiometry of La_2CoO_4 to clarify the reported results by J.T. Lewandowski *et al.* [7], and determine the phase stability range of La_2CoO_4 at 900°C and 1100°C. Samples containing La_2CoO_4 phases will be synthesised from different La:Co ratios using the nitrate freeze-drying method and then heat treated at two temperatures; 900°C and 1100°C. The samples will be investigated and the La:Co ratio of the La_2CoO_4 phase will be determined using XRD, EPMA-WDS, and TEM-EDS.

1.2.1 This study

All experimental work performed in this study were carried out at the laboratory of Professor Uda at Kyoto University. All necessary equipment and chemicals was provided from his laboratoy. The synthesis of the samples was perfomed by the author of this thesis and the XRD and EPMA measurements were performed in cooperation with master students Katsuhiro Ueno and Katou Kouhei of Kyoto University.

Chapter 2

Background

In this chapter, some of the earlier work regarding the nonstoichiometry of La_2CoO_4 will be presented. Most focus will be given to the paper written by Lewandowski *et al.* [7] which reported a lanthanum deficiency in the La_2CoO_4 oxide. In this thesis, the work will be performed to clarify if any lanthanum deficiency exists in this oxide, so this paper is an important source of information.

There has been some disagreement about the stoichiometry of the compound La_2CoO_4. Earlier research of the compound has been done, and a broad range of lattice parameters have been observed, which indicates a variation in composition. While there is an agreement that the compound deviate from stoichiometric values, there is a disagreement of how the compound deviates from stoichiometry.

2.1 Nonstoichiometric K_2NiF_4-type phases in La-Co-O-system by Lewandowski *et al.*

In the work of Lewandowski *et al.* the objective was to determine the lanthanum deficiency, oxygen stoichiometry and determine the cobalt oxidation state for the La_2CoO_4-type phases in the La-Co-O system [7]. They wanted to investigate the structural chemistry of this phase based on earlier work which had reported various lattice parameters and cobalt with different oxidation states. The data supported that the La_2CoO_4 phase did not have a stoichiometric composition and suggested the more fitting formula $La_2CoO_{4+\delta}$ to explain the different

oxidation states of cobalt. This formula was not likely according to Lewandowski *et al.* [7] due to the densely packed K_2NiF_4-structure and meant that lanthanum deficiency in the phase was a better description of the reported data.

In their work they prepared several samples with La:Co ratio from 1.7:1 to 2.0:1 which were slowly heated to 1000 °C at a low partial oxygen pressure for 120 hours [7]. XRD confirmed that La_2CoO_4 was the major phase in all samples but with various lattice parameters. Low-temperature oxidation of all samples gave one single La_2CoO_4-phase with no variations in lattice parameters. Comparing the XRF and XRD analysis after low-temperature oxidation indicated that the La:Co ratio of the La_2CoO_4-phase was close to 1.85 where a single phase occurred. Lower or higher La:Co ratio led to a multiphase product. The results from XRF and XRD analysis are presented in Table 2.1. Based on the results of the low-temperature oxidation the ideal formula for the oxidised form would be $La_{1.83}Co^{III}_{0.5}Co^{II}_{0.5}O_4$.

Table 2.1: Results from XRF and XRD analysis. The table is taken from [7].

La/Co ratio (XRF)	Second phase (XRD)
1.71	CoO
1.75	Slight CoO
1.79	Trace CoO
1.85	
1.92	Trace $La_2O_2CO_3$
2.01	$La_2O_2CO_3$

Thermogravimetric experiments of this oxidised form in lower partial oxygen pressure gave the discovery of a metastable fully reduced form $La_{1.83}CoO_{3.75}$ only containing divalent cobalt [7]. Thermogravimetry with a controlled partial oxygen pressure did identify a third form of this phase being an intermediate of the fully oxidised and fully reduced form, having the ideal formula $La_{1.83}Co^{III}_{0.25}Co^{II}_{0.75}O_{3.875}$. At more oxidising conditions the lattice parameters of this partially reduced form will vary with increasing content of Co^{III} until the fully oxidised form is reached. Figure 2.2 presents the lattice parameters for the different $La_{1.83}CoO_{4-x}$ phases reported in this paper.

Table 2.2: Lattice parameters for the $La_{1.83}CoO_{4-x}$ phases reported by Lewandoski *et al.* [7].

Ideal formula	a [nm]	b [nm]	c [nm]	V [nm]
$La_{1.83}CoO_4$ (x=0)	0.5538(5)	0.5475(5)	1.257(1)	0.3810
$La_{1.83}CoO_{3.875}$ (x=0.125)	0.5550(5)	0.5484(5)	1.267(1)	0.3856
$La_{1.83}CoO_{3.75}$ (x=0.25)	0.5606(5)	0.5471(5)	1.265(1)	0.3880

When reduced further, $La_{1.83}CoO_{3.875}$ separates into a two-phase mixture consisting of $La_{1.83}CoO_{3.875}$ and $La_{1.83}CoO_{3.375}$ before a single phase of the fully reduced is obtained as $La_{1.83}CoO_{3.375}$.

2.2 Other research of La_2CoO_4

Because of the interest in oxides with K_2NiF_4 structure, and the lack of satisfactorily charachterisation and description of the oxide La_2CoO_4 Ram *et al.* carried out syntesis and characterisation of the oxide [8]. The work previously done regarding La_2CoO_4 had so far given varying results which should be clarified. Two $La_2CoO_{4+\delta}$ samples were prepared by skull melting and by the ceramic method and stoichiometric La_2CoO_4 was prepared in a dilute hydrogen atmosphere. The La:Co ratio of all samples was measured to be 2:1 within an experimental error. To confirm the reported lanthanum deficient structure $La_{1.83}CoO_{4-x}$ by Lewandowski *et al.*, the structure was attempted to be prepared, but the attempt always resulted in a mixture of La_2CoO_3 and CoO. The results reported indicated that all prepared La_2CoO_4 phases had a stoichiometric cation ratio. However the lattice parameters reported, presented in Table2.3 are close to the values reported by Lewandowski *et al.*, shown in Table 2.2, for the lanthanum deficient compound.

Table 2.3: Unit cell parameters of La_2CoO_4 reported by Ram *et al.* [8].

Composition	a [nm]	b [nm]	c [nm]
$La_2CoO_{4.10}$	0.5543(3)	0.5493(3)	1.2684(10)
$La_2CoO_{4.11}$	0.5526(3)	0.5476(5)	1.2650(10)
La_2CoO_4	0.5614(3)	0.5474(3)	1.2648(10)

In the thermogravimetric study of the La-Co-O system performed by K. Kitayama the phase stability of the system was established at 1100 °C and 1150 °C as a function of the oxygen partial pressure [9]. From the work no lanthanum deficient composition was found, but the compostion La_2CoO_4 was reported. This result was consistent with his earlier thermogracimetric studies of the system at 1200 °C [10].

Chapter 3

Theoretical background

In this chapter, an overview of some theoretical background will be given which is beneficial to the work performed in this study. Firstly an introduction of fuel cells will be presented, along with a more detailed presentation of solid oxide fuel cells, since this is an application La_2CoO_4 and similar compounds are of interest. Then theory related to the crystal structure, phase stability and nonstoichiometry of La_2CoO_4 will be presented.

3.1 Fuel cells

3.1.1 Introduction and operation

Fuel cells are devices which convert chemically free energy, stored in the reactants, directly to electrical energy [11]. The first fuel cell was invented in 1839 by William Grove by reversing the water electrolysis and generating energy from hydrogen and oxygen. Today the fuel cell design has improved greatly from Grove's fuel cell design which was made up of dilute sulphuric acid with platinum electrodes. However, it was not until almost a century later that fuel cells found a practical application within space travel by NASA. It was the alkaline fuel cell invented by Francis Bacon that was used to create energy and water for the astronauts [11]. Now fuel cells can be found used in everyday life, but the fuel cells have still not achieved commercial success on any significant scale.

The concept of a fuel cell is similar to that of a battery, only the fuel is continuously supplied to the cell [12]. While there are many different fuels that can be used, in the simplest case hydrogen is used as fuel and the reaction occurring is:

$$H_2 + \frac{1}{2}O_2 \rightarrow H_2O \tag{3.1}$$

The reactants are separated by an electrolyte to avoid chemical recombination of the reactants. This electrolyte will have a high conductivity of specific ions. When the fuel cell is in operation, it will conduct a current of ions equivalent to the electric current passing through the external current. In addition to the electrolyte, a fuel cell also consists of an anode and a cathode, both being electro-catalytically porous electrodes. Figure 3.1 show the electrochemical process that is occurring in a fuel cell. The reactions occur at the interface between the electrodes and the electrolyte. In most cases, the fuel gets oxidised at the anode creating protons and free electrons. The protons will pass through the electrolyte, while the electrons pass through an external circuit generating electricity, to the cathode. When the protons reach the cathode they will combine with the electrons and oxygen forming water.

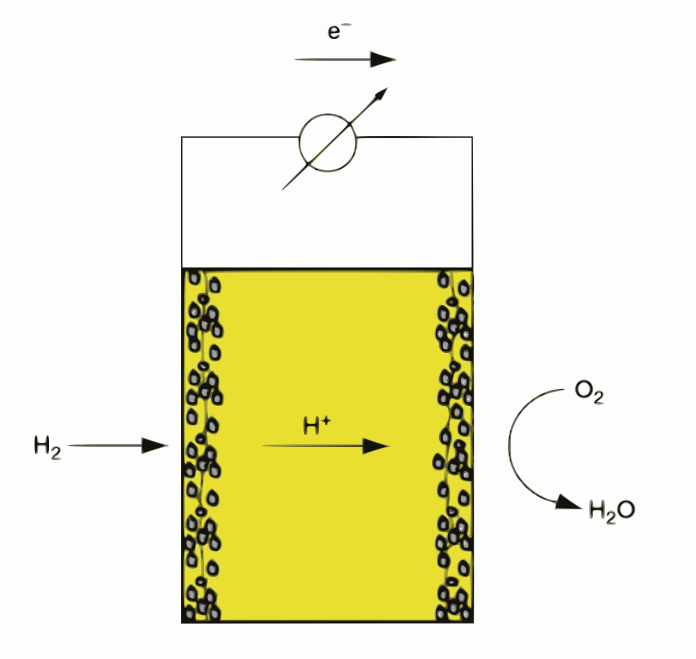

Figure 3.1: Schematic illustration of the electrochemical process of a fuel cell. The illustration is reprinted from [4].

Unlike the commonly used combustions engines, fuel cells are not restricted by the Carnot cycle and have therefore a higher potential for achieving a high-efficiency rate [4]. In theory, it is possible for the efficiency of a fuel cell to be higher than unity, though in practice the efficiency lies below unity since irreversible losses happen in almost every part of a fuel cell. Despite this, fuel cells have shown to have an efficiency of 50% in small scale experiments, showing that the high efficiency is scaleable. This is not the case for combustion engines that can only be most efficient a certain minimum engine size [12, 13]. The fuel cells ability to achieve high efficiency at any scale makes them good contenders against combustion engines, especially in the transport section. Their high efficiency can reduce the consumption of primary energy and can reduce the CO_2 emission because fuel cells emit zero or very low emissions [11].

3.1.2 Solid oxide fuel cell (SOFC)

Different fuel cells are defined after what type of material the electrolyte substance is made up of since it is a significant part of the fuel cell design. In the solid oxide fuel cell (SOFC) the electrolyte is made of a ceramic or solid oxide, with yttria stabilised zirconia being the most common [13]. Since the SOFC only consists of solid parts, it is not restricted by the conventional plane design and can be designed as tubes, and the materials are not susceptible to corrosion since no liquid is present. Unique for the SOFC is that the electrolyte conducts oxygen ions from the cathode to the anode. This differs from the typical electrochemical process described in Section 3.1.1. The oxygen ions will react with the hydrogen at the anode and form water. Since the electrolyte conducts oxygen ions, the SOFC has a lot of fuel flexibility, which means that natural gas and even carbon can be used as fuel [14]. Figure 3.2 shows a sketch of the operation of an SOFC.

The solid oxide material used as an electrolyte in SOFCs has a high activation energy for conductivity, which makes the lower limit for the operation temperature high (>800°C) [2]. The high operating temperature contributes to the high efficiency that SOFC produces. Since the operating temperature is greater than the reforming temperature, the excess heat can go to this process. Also, the excess heat can be used to drive a gas turbine generating electricity, increasing the efficiency [15]. There are several applications where SOFC is well suited. One example is in combined heat and power applications, such as individual households where

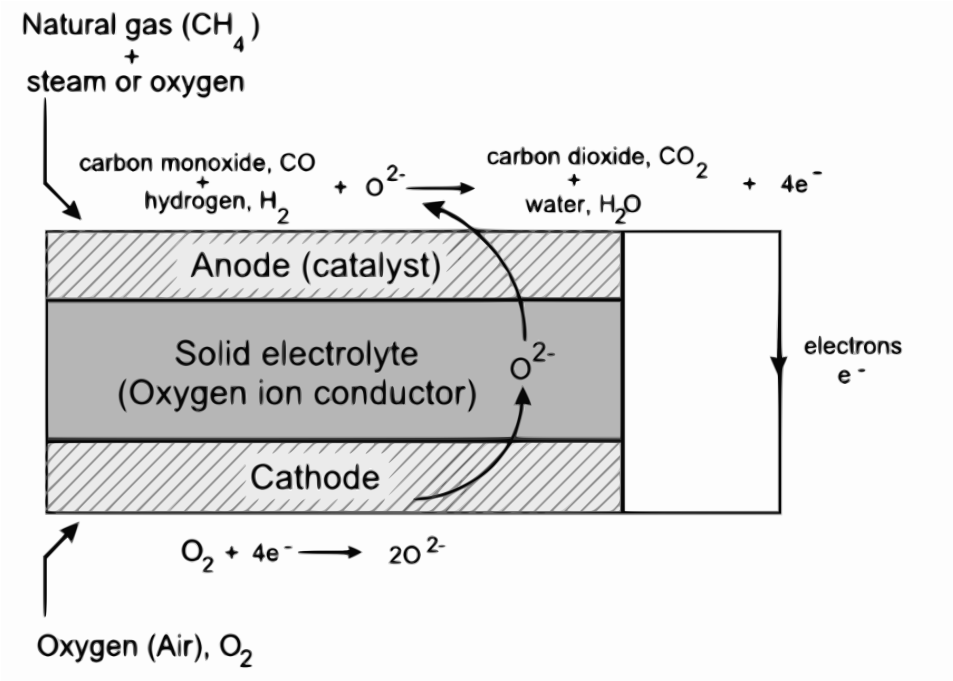

Figure 3.2: Illustration showing the operating principle of a solid oxide fuel cell. The illustration is reprinted from [15].

hot water and electricity will come from one system. This will be more efficient compared to getting electricity from a local power plant and hot water from the house water boiler unit.

Other than the high efficiency, there are several other advantages to the SOFC such as the long-term stability, fuel flexibility, low emissions, and relatively low cost. Still, the largest disadvantage of the SOFC is the high operating temperature which leads to a long start up time and mechanical and chemical issues. Therefore, much research is done to reduce the operating temperature of SOFC (<650°C). By lowering the operating temperature, it will allow a broader set of materials to be used in SOFC applications. A drawback of reducing the temperature is that the electrolyte conductivity and electrode kinetics will be reduced and it necessary to find alternative cell materials and other designs to solve these issues [3].

Several materials are studied extensively for their potential to be used in SOFC applications. La_2CoO_4 and similar compounds such as La_2CoO_4 have shown properties suitable for the use as a cathode material [16–18]. Interest in these materials is because of their good conductivity and availability to transport oxygen. Much research focuses on finding cathode materials with high rates of oxygen transport because the cathode efficiency reduces significantly when the operating temperature is reduced.

3.2 Crystal structure

In ternary compounds there are three ionic species present, creating several structural possibilities the compound can have. The perovskite structure is the most common structure found in ternary compounds with the formula ABO_3 [19]. The perovskite structure has a cubic unit cell with every A cation being surrounded by 12 O^{2-} anions, while every B cation being surrounded by six O^{2-} anions. La_2CoO_4 have the perovskite-like structure K_2NiF_4 consisting of alternating layers of perovskite sheets (ABO_3) and rock salt (AO) layers along the c-axis. A comparison of the perovskite structure and the structure of La_2CoO_4 is shown in Figure 3.3.

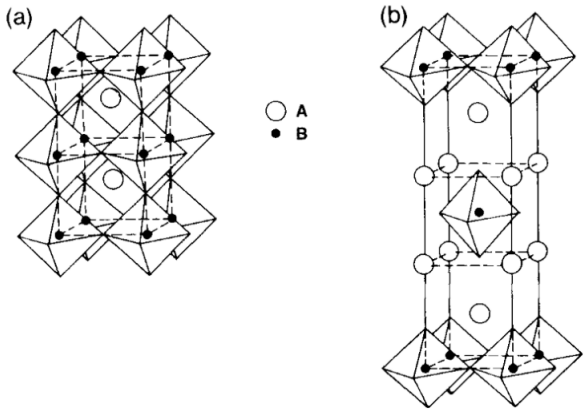

Figure 3.3: Crystal structure of a) Perovskite and b) A_2BO_4. The illustration is reprinted from [7].

The La_2CoO_4 compound is described to have an orthorhombic structure at room temperature. With increasing temperature the crystal structure of La_2CoO_4 changes into a secondary orthorhombic phase at approximately 413 K, before transforming into a tetragonal phase at 433K [20].

3.2.1 Ruddlesden-Popper series

The La_2CoO_4 compound is a member the Ruddlesden-Popper series which consists of compounds with the formula $AO(ABO_3)_n$, where A is a cation from the alkali, alkali earth or rare earth metals and B is a cation transition metal. All Ruddlesden-Popper structures have a similar structure to the K_2NiF_4 structure described above with layers of perovskite $(ABO_3)_n$) interleaved with sodium chloride (AO) layers [2]. The series is named after S.N. Ruddles-

den and P. Popper who first described the structure in 1957 [21,22]. The perovskite structure can be described as a Ruddlesden-Popper structure with n=∞. In addition to the La_2CoO_4 compound, the ternary compounds $La_4Co_4O_{10}$ and $LaCoO_3$ in the La-Co-O system are also members of the Ruddlesden-Popper series.

3.2.2 Lattice parameters

As mentioned earlier La_2CoO_4 adopts both orthorhombic and tetragonal crystal structures depending on the temperature. In this work, La_2CoO_4 will only be analysed and characterised at room temperature when the compound has an orthorhombic structure.

The orthorhombic unit cell is described by three distinct lattice parameters; a, b and c. The atoms and ions in the lattice lie in different lattice planes [23]. Every lattice plane is a member of a set of parallel planes with a constant distance between them. The lattice planes can be uniquely defined by the Miller indices h, k and l usually written as (hkl). The interplanar distance, d, between the atomic layers in the crystal is related to the Miller indices and the lattice parameters of an orthorhombic compound through Equation 3.2.

$$\frac{1}{d_{hkl}^2} = \frac{h^2}{a^2} + \frac{k^2}{b^2} + \frac{l^2}{c^2} \tag{3.2}$$

When radiation of a certain wavelength, λ, is applied to the crystal (1.5418 Å in this study), as in XRD characterisation, the reflection from two adjacent parallel planes of atoms separated by the distance d will interfere constructively at a certain angle, θ [19]. The relationship between d, λ and θ is given by Bragg's law shown in Equation 3.3.

$$2\text{d}\sin\theta = n\lambda \tag{3.3}$$

3.3 Phase stability

The La-Co-O system consists of several ternary and binary compounds in which the phases depend on the temperature and oxygen partial pressure of the surroundings. In his work Kitayama established the phase equilibria of the system at 1100 °C and 1150°C by changing the oxygen partial pressure from 0 to 12.00 in -log(p_{O_2}/atm) where La_2O_3, CoO, La_2CoO_4, $LaCoO_3$ and $La_4Co_3O_{10}$ are present [9]. In his previous work, the phase equilibria have been determined at 1200°C. From the work performed he reported the standard Gibbs free energy of the reactions in the phase diagrams of the La-Co-O system and confirmed their linearity with temperature under the experimental conditions used.

In the La-Co-O system there are three ternary compounds; La_2CoO_4, $La_4Co_3O_{10}$ and $LaCoO_3$ with their mean valencies of cobalt ions being +2, +2.67 and +3, respectively [24]. As the partial oxygen pressure increases the ternary compound with the higher cobalt ion valency tends to be preferred [6, 24, 25]. This tendency can be seen in the isothermal phase stability diagram shown in Figure 3.4 reported by Seppänen *et al.* [6] as part of their work on the stability of the ternary phases in the La-Co-O system. In the study the stability of the ternary phases as a function of the temperature in the range 1175-1325K was measured. Using emf measurements the change in Gibbs free energy, $\Delta G°$, for the equilibria reactions in the La-Co-O system was found as a function of the temperature. The experimental work indicated a linearity between the standard Gibbs energy of the reactions, the same result as reported by Kitayama [9].

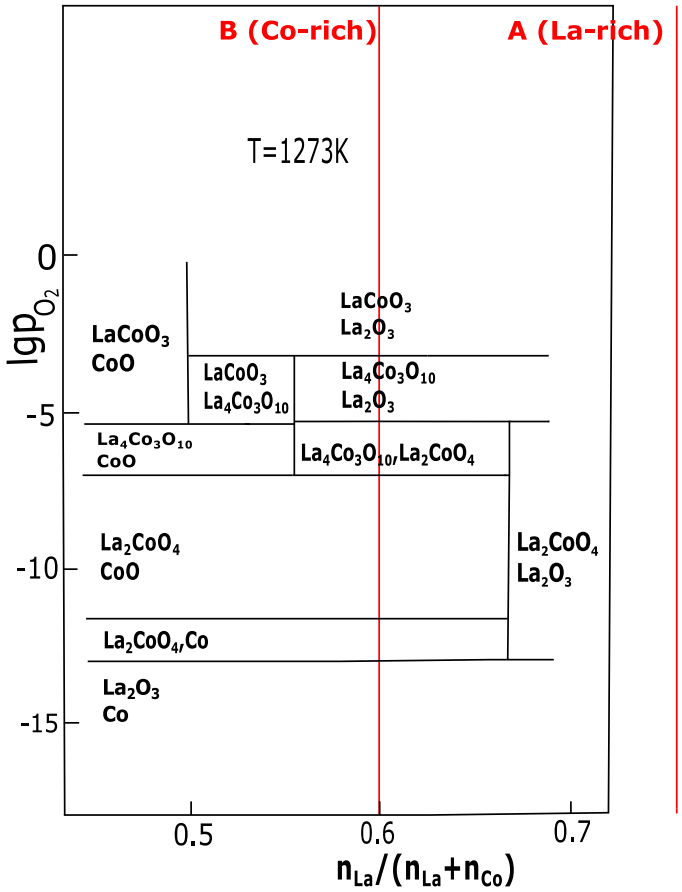

Figure 3.4: The isothermal stability diagram for the system La-Co-O at 1273K. (p_{O_2}/bar) The diagram is adapted from Seppänen *et al.* [6].

The diagram shows the homogeneity range of the ternary phases approximated as lines due to the range not being exactly known [6]. To determine if La_2CoO_4 has any homogeneity range and nonstoichiometry, analysis of samples having a La:Co ratio lower and higher than the approximated line in Figure 3.4 can be carried out. The red lines in Figure 3.4 represent the La:Co ratios of samples A and B that will be examined in this thesis and are equal to 75:25 and 60:40, respectively.

As mentioned earlier, research has shown that the standard Gibbs energy of the reactions in the La-Co-O system is linearly dependent on the temperature. In the work performed in this study the samples will heat treated at 1100°C and 900 °C, so the phase diagram at these temperatures will not be the same as the one presented in Figure 3.4. However, the change in the standard Gibbs energy due to temperature change is not too large in this temperature range, causing the phase stability diagram to look close to the one for T = 1273K. In Figure 3.5 an isothermal stability diagram for the La-Co-O system at T = 1373K is shown, and it can be seen that the two phase diagrams that the relationship are basically the same.

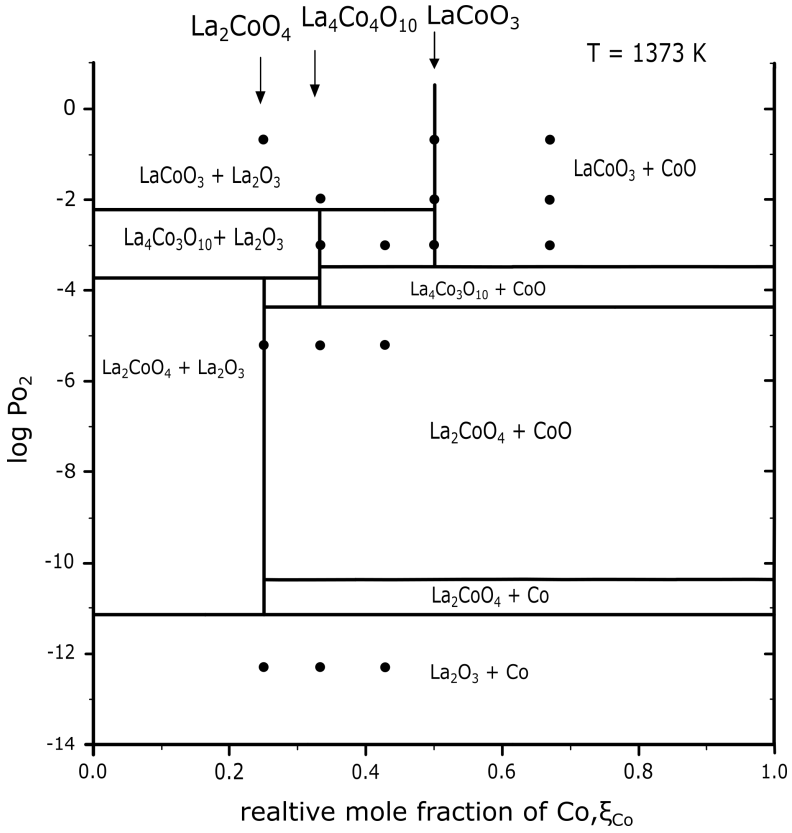

Figure 3.5: Isothermal phase diagram for the La-Co-O system at 1373K, (p_{O_2}/atm). The diagram is reprinted from Petrov *et al.* [26].

The stability of La_2CoO_4 is dependent on the partial oxygen pressure, so it is necessary to control the partial oxygen pressure during the synthesising of the compound to achieve the correct phase composition. From Figure 3.4 it can be seen that Sample A will have the phases; La_2CoO_4 and La_2O_3 while Sample B will have the phase La_2CoO_4 with either Co,CoO or La_2CoO_4 depending on the partial oxygen pressure. From Figure 3.4 it can be seen that the p_{O_2} for the Co/CoO equilibrium lies around 10^{-12} bar. Ar gas flow can be used to lower p_{O_2} to lie within the stability range of La_2CoO_4, but it may contain a partial oxygen pressure of 10^{-5} atm (p_{O_2} in flowing Ar gas have been measured earlier, and may come from the air). Therefore using Co metal as an oxygen absorber, p_{O_2} can be controlled to be within the stability range of La_2CoO_4.

3.4 Point defects and nonstoichiometry

Inorganic compounds were earlier believed to have stoichiometric compositions and that their atoms are arranged in an ideal structure where all sites are occupied [5]. However, in the last century, it has been common to assume that many inorganic compounds have varying compositions, and stoichiometric compositions can only be obtained at certain partial pressures at the given temperature.

3.4.1 Point defects

All compounds above the absolute zero temperature contain some defects because up to a certain concentration they reduce the Gibbs free energy, ΔG [27]. While the formation of defects requires energy, ΔH the defects also introduce disorder in a perfect crystal, increasing the change of entropy, ΔS, which is defined by the Boltzmann equation:

$$S = k \ln W \tag{3.4}$$

where k is a constant and W is the probability of possible position a defect can have. The probability will be high at small concentrations of defects because the defects can occupy many positions. Therefore, the entropy term in Equation 3.5 will be larger than the enthalpy term, decreasing the ΔG.

$$\Delta G = \Delta H - T\Delta S \tag{3.5}$$

The simplest form of defects found in a crystal are the two types of point defects; vacancies, where an atom is missing from the lattice site, and interstitials, where an atom is placed in a normally unoccupied site in the crystal structure [28]. In a pure crystal, intrinsic defects can be found such as Schottky defects and Frenkel defects, where ions with the opposite charge leave their lattice site, and an atom changes its position from a lattice site to an interstitial site, respectively. These defects maintain the electron neutrality in the compound and only give minimal deviations from the stoichiometric compositions, unlike defects caused by reactions with the surrounding atmosphere.

3.4.2 Nonstoichiometry

Greater deviations from the stoichiometric composition occur when oxides react with the oxygen in the atmosphere [29]. When oxides are in contact with the vapour of its components, the composition of the solid phase will be dependent on the concentration of the component in the vapour phase because a thermodynamic equilibrium will exist between the phases. When a solid phase and vapour phase are in equilibrium ($\Delta G=0$) at a specific temperature and pressure, any change in pressure will change the composition if the energy of activation at that specific temperature is high enough. Nonstoichiometric compounds will usually have a range in composition but will retain the same structure [30]. In the case of La_2CoO_4, any nonstoichiometric version of this substance will have the same K_2NiF_4 structure. An important criterion for a nonstoichiometric compound is that the lattice parameters need to have a smooth change over the composition range, which is known as Vegard's rule [19]. A discontinuity in the lattice parameter value is an indication of a formation of a new crystal phase.

The ratio between cation and anion lattice sites will be the same regardless if the compound is stoichiometric or not [29]. To preserve the electroneutrality, electronic defects must be present by having ions with different valence states in the crystal. Large deviations from stoichiometry are often observed in oxides which contain cations that can exist in several valence states in the crystal [31]. This can be observed in iron oxide in which nonstoichiometry often occur, by having iron present as both divalent and trivalent, causing Fe^{2+} vacancies to form to maintain the electroneutrality. Figure 3.6 shows a schematic illustration of the phenomenon in $Fe_{1-x}O$. Therefore nonstoichiometry is usually found in transition metal oxides, lanthanide oxides, and the actinide oxides. In the case of La_2CoO_4, cobalt has been found to have different valence states, Co^{2+} and Co^{3+}, indicating nonstoichiometry in the compound.

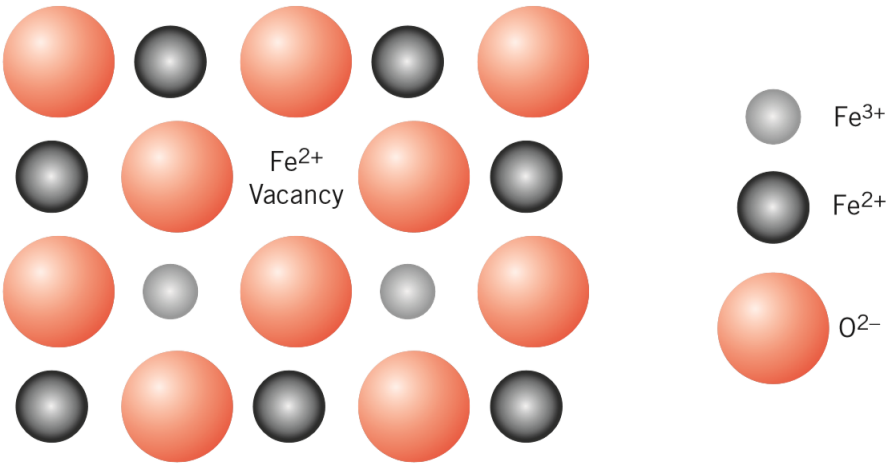

Figure 3.6: Schematic illustration of nonstoichiometry in $Fe_{1-x}O$. The figure is reprinted from [31].

Nonstoichiometry in oxides is usually explained and classified into four groups; Oxygen-deficient oxides, oxides with excess oxygen, metal-deficient oxides and oxides with excess metal [29].

1. **Oxides with excess metal** occur when the oxygen partial pressure over the crystal is lower than the equilibrium value for a stoichiometric composition. Oxygen ions in the crystal will transfer to a gaseous state leaving an excess of metal atoms or lower-valent ions in interstitial positions.

2. **Oxygen-deficient oxides** occur under the same conditions as mentioned above, but oxygen sites are left vacant when the oxygen ions transfer to a gaseous phase instead.

3. **Oxides with excess oxygen** occur when the oxygen partial pressure above the crystal is higher than the equilibrium value for a stoichiometric composition. The oxygen in the air will react with the oxide leaving oxygen ions in the interstitial positions in the crystal structure.

4. **Metal-deficient oxides** occur under the same conditions mentioned above when no suitable interstitial positions are available. The excess of oxygen ions can build on the normal lattice sites, creating new oxygen lattice sites and an equivalent of vacant metal sites which will diffuse into the crystal.

The stoichiometric compound, La_2CoO_4 will only contain divalent cobalt ions. However, as mentioned earlier, La_2CoO_4-phases have been found with both divalent and trivalent cobalt

ions, indicating that the phases are nonstoichiometric. Earlier authors have suggested that the presence of trivalent cobalt is explained by La_2CoO_4 having the ability to obtain an excess of oxygen by leaving oxygen ions in interstitial positions which is shown in the following equation [18]:

$$La_2CoO_4 + \frac{x}{2}O_2 \rightarrow La_2CoO_{4+x} \tag{3.6}$$

In the case of ternary oxides, it is also possible for nonstoichiometry to exist between the cations in the compound [32]. Cation nonstoichiometry can usually be achieved by synthesises but may also occur naturally. This cation-cation nonstoichiometry is of interest because ternary oxides exhibit important material properties such as ferroelectricity, piezoelectricity and magnetic properties which can be affected by the cation nonstoichiometry of the compound. Lewandowski *et al.* [7] suggested based on their work that the stoichiometric composition La_2CoO_4 did not exist. The work indicated that K_2NiF_4 phase was lanthanum deficient with 1/12 lanthanum sites vacant, and the cation stoichiometry is not stoichiometric but has the La/Co ratio equal to 1.83. The fully oxidised material will contain about 50% trivalent cobalt and have the formula $La_{1.83}CoO_4$. Because this proposed formula with a cation nonstoichiometry will lose lattice oxides as the trivalent cobalt reduces to divalent cobalt, shown in Equation 3.7, the compound will be described as an oxygen-deficient oxide.

$$La_{1.83}CoO_4 \rightarrow La_{1.83}CoO_{4-x} + \frac{x}{2}O_2 \tag{3.7}$$

From this, it can be seen that the type of oxygen nonstoichiometry in La_2CoO_4 is dependent on whether or not the compound has cation nonstoichiometry. The different possibilities give different mechanisms of which the nonstoichiometry can be described, and since nonstoichiometry affects the properties of the material, it is important to determine the right situation for this compound.

Chapter 4

Experimental

The experimental work conducted in this thesis include synthesising mixtures including La_2CoO_4 from different La:Co ratios at various heat treatment conditions and characterisation and analysis to confirm the desired phases and determine the composition of the La_2CoO_4 phase. Included in the work is also low-temperature oxidation of specific samples, followed by characterisation to determine if any changes in the phase composition and in the lattice parameters occurred.

4.1 Synthesis of La_2CoO_4-containing mixture

The synsthesis of samples containing a La_2CoO_4-phase is performed in two steps. In the first step a precursor powder containing mixed oxides is prepared, described in Section 4.1.1. In the second step the the precursor powder is heat treated to achieve the desired phases, described in Section 4.1.2.

4.1.1 Preparation of precursor powder

Aqueous solutions of 1M La^{3+} in HNO_3 and 1M La^{2+} in HNO_3 were prepared from $La(NO_3)_3 \cdot 6\,H_2O$ and 1M $Co(NO_3)_2 \cdot 6\,H_2O$, respectively. The solutions were used to create a La-rich solution with a La:Co ratio of 75:25 and a Co-rich solution with a La:Co ratio 60:40 named samples A and B, respectively. Table 4.1 shows some details of the chemicals used.

Table 4.1: Chemicals used to create precursor solutions.

Chemical	**Formula**	**Purity [%]**	**Supplier**	**CAS**
Lanthanum(III) nitrate hexahydrate	$La(NO_3)_3 \cdot 6H_2O$	99.9	Wako	10277-43-7
Cobalt(II) nitrate hexahydrate	$Co(NO_3)_2 \cdot 6H_2O$	99.5	Wako	10026-22-9

Using the nitrate freeze-drying method 50 ml of the solutions A and B were atomised. A mist of the solutions was created using an ultrasonic spray nozzle and was directly frozen by letting the mist fall into liquid nitrogen which was continuously stirred using a magnetic stirrer. The frozen particles were then vacuum-dried in a freeze dryer (DRC-1100 and FDU-2100, EYEA) under vacuum at a temperature of -40°C. A thermocouple was used to control the temperature of frozen solution. The temperature was gradually increased over two days until room temperature, and the powders were dry. The product of this process was (La, Co)$NO_3 \cdot nH_2O$. The samples were transferred into crucibles and heat treated in a vertical furnace at 600°C under vacuum for 10 hours to create the precursor powders consisting of mixed oxides. Cobalt (Co: 99%, Nacalai Tesque inc.) was present as a oxygen absorber to control the oxygen partial pressure in the furnace during the heat treatment. Figure 4.1 shows a schematic overview of the synthesis of the precursor powder.

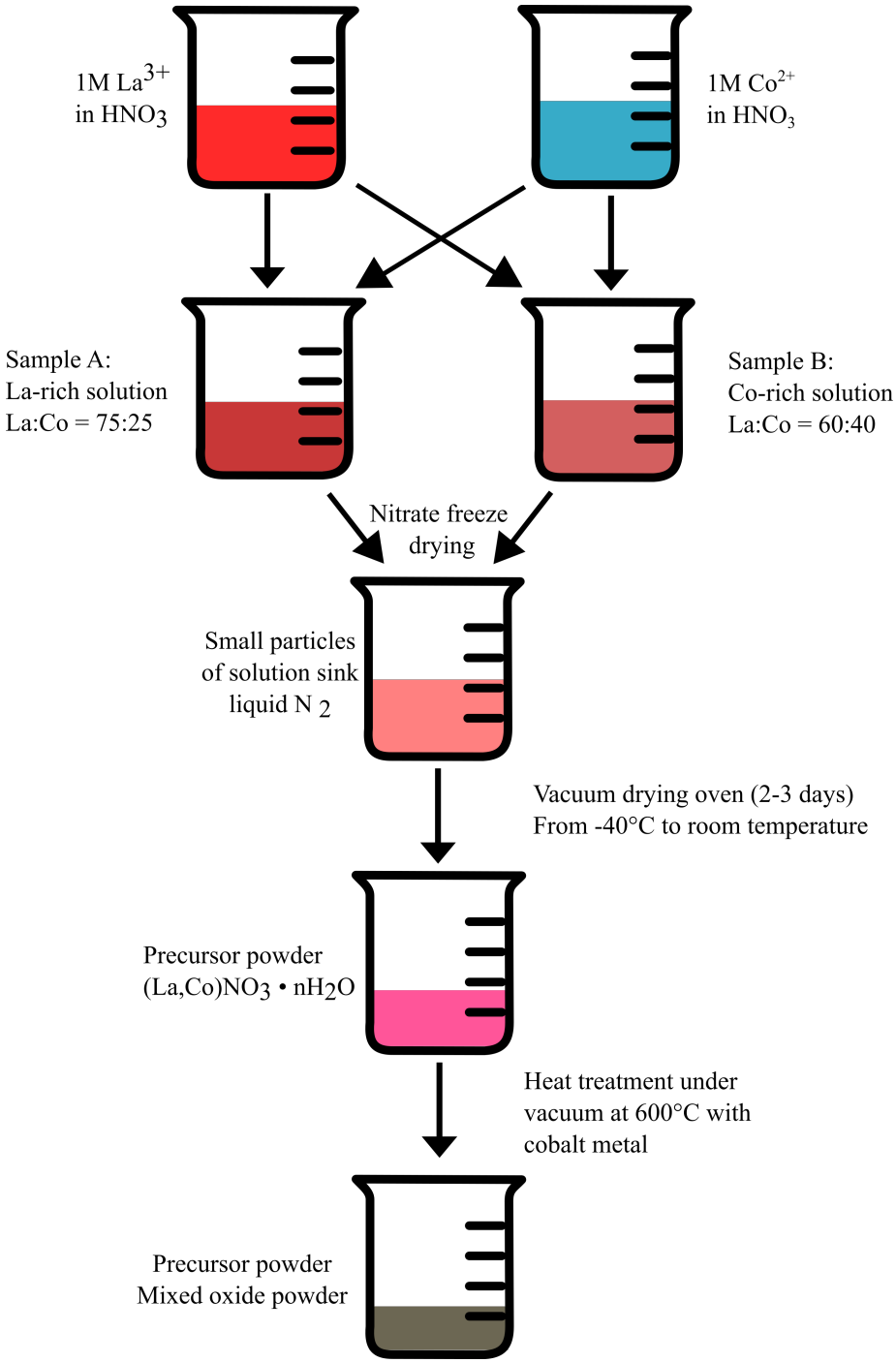

Figure 4.1: Schematic overview of the synthesis of the precursor mixed oxide powder of samples A and B. 1M solutions of La^{3+} and Co^{2+} in NO_3 were mixed into two mixtures with varying La:Co ratio. Particles of the solutions were created using the nitrate freeze-drying technique before being vacuum dried. The powders were then heat treated under vacuum at 600°C to create the mixed oxide powders.

4.1.2 Heat treatment conditions

The precursor powders of samples A and B were heat treated at 1100 °C, referred to as samples A1 and B1, and at 900°C, referred to as samples A2 and B2. All samples were heat-treated in an argon flow atmosphere. The samples were placed inside an alumina ring inside an alumina crucible. 20 g of cobalt was put outside the alumina ring as a oxygen absorber to control the partial oxygen pressure during the heat treatment to obtain the correct phases and avoid unwanted phases. The sample sizes used was 0.5 g and 1 g of samples A and B, respectively. Figure 4.2 shows the crucible used with the alumina lid (Figure 4.2a) and the inside of the crucible (Figure 4.2b).

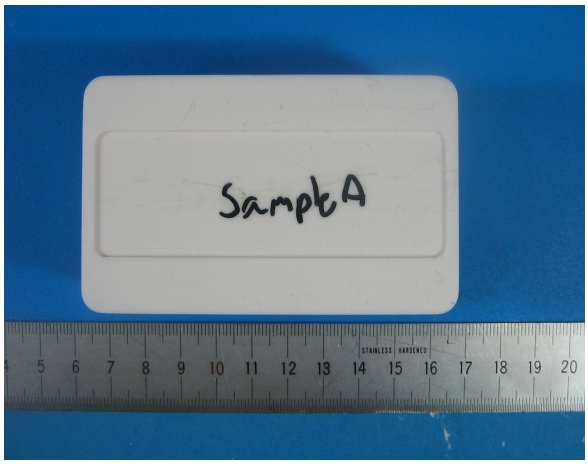

(a) Crucible with the alumina lid.

(b) Inside of crucible. Sample powder lies inside an alumina ring with cobalt surrounding the outside.

Figure 4.2: Image of crucible containing Sample A after heat treatment at 900°C.

The samples were heat treated at sintering temperatures of 1100°C for 10 hours and 900°C for 120 hours in a tubular furnace. The heating rate was 250°C/h up to 1000°C and 200 °C/h up to 1100 °C with the cooling rate being the reverse. The furnace was evacuated to 10 Pa before being filled with argon gas. Table 4.2 shows a summary of the samples La:Co ratio and heat treatment conditions.

Table 4.2: Summary of the samples preparation.

Sample	La:Co ratio	Heat treatment	Hours
A1	75:25	1100 °C	10 h
A2	75:25	900 °C	120 h
B1	60:40	1100 °C	10 h
B2	60:40	900 °C	120 h

4.2 Low-temperature oxidation

To investigate the possibility of secondary phases the samples were oxidised at a low temperature in ambient air. 300 mg of samples A1 and B1 were measured out and placed in alumina crucibles. The samples were heated in a furnace at a heating rate of 300°C/h to 600 °C for 100 hours.

4.3 Synthesis of $LaCoO_3$ standard sample

A standard sample containing stoichiometric $LaCoO_3$ was prepared to correct potential systematic errors in the data obtained from the EPMA analysis.

The solution with a La:Co ratio equal to 1:1 was prepared from the aqueous solutions containing 1M La^{3+} in HNO_3 and 1M La^{2+} in HNO_3 prepared earlier. The precursor powder was synthesised using the same technique used to synthesise the precursor powders to samples A and B described in Section 4.1.1. No cobalt was present when the powder was heat treated at 600°C.

The powder was pressed into a pellet under a uniaxial pressure of 500 MPa using a Desktop Newton Press NT-100H. The pellet was heat treated at 1300°C for 24 hours in ambient air. The heating rate was 250°C/h up to 1000 °C and 200°C/h up to 1300°C. The crucible lid was not used during heat treatment to ensure a good supply of oxygen to the samples.

4.4 Characterisation and analysis

In this work, the phase composition of the samples was characterised using X-ray diffraction (XRD). Analysis of the La:Co ratio of the La_2CoO_4 phases has been performed using electron probe microanalyser (EPMA) and EDS using a transmission electron microscope (TEM-EDS). Details of the instruments used and the sample preparations are described in this section.

4.4.1 X-ray diffraction (XRD)

X-ray diffraction was performed using X'pert proMPD PANanalytical with Cu Kα radiation, to identify the phases in the samples. All measurement were carried out at room temperature. An X-ray diffractogram was obtained by scanning in the 2θ-range from 10° to 90° with a step size of 0.0167°. The phases present were identified using PANanlytical X'pert Highscore software.

Rietveld refinement based on the X-ray diffractogram was performed using the PANanlytical X'pert Highscore software to determine the lattice parameters.

4.4.2 Electron probe microanalyser (EPMA)

Composition analysis of the samples was performed using JEOL JXA-8530F. Wavelength-dispersive X-ray spectroscopy (WDS) was carried out to analyse the composition of the samples. Images of the samples were taken using backscattering and secondary electrons. The powder samples were carbon coated using a carbon coater (CADE-E) to achieve good conductivity and avoid charge build up on the samples.

4.4.3 TEM-EDS

Composition analysis of the samples was performed using JEM-2100F Field emission electron microscope. The samples were prepared by dissolving the samples in 96% ethanol. A small amount of the powder was left on the sample holder after the ethanol had evaporated.

Chapter 5

Results

5.1 Standard sample containing $LaCoO_3$

A sample containing the phase $LaCoO_3$ with the La:Co ratio equal to 1:1 was prepared as a standard sample. The pellet was characterised using XRD to identify the phases present. The X-ray diffractogram is presented in 5.1. The peaks in the diffraction pattern are directly below the purple symbol which indicates that $LaCoO_3$ is the only phase present in the standard sample.

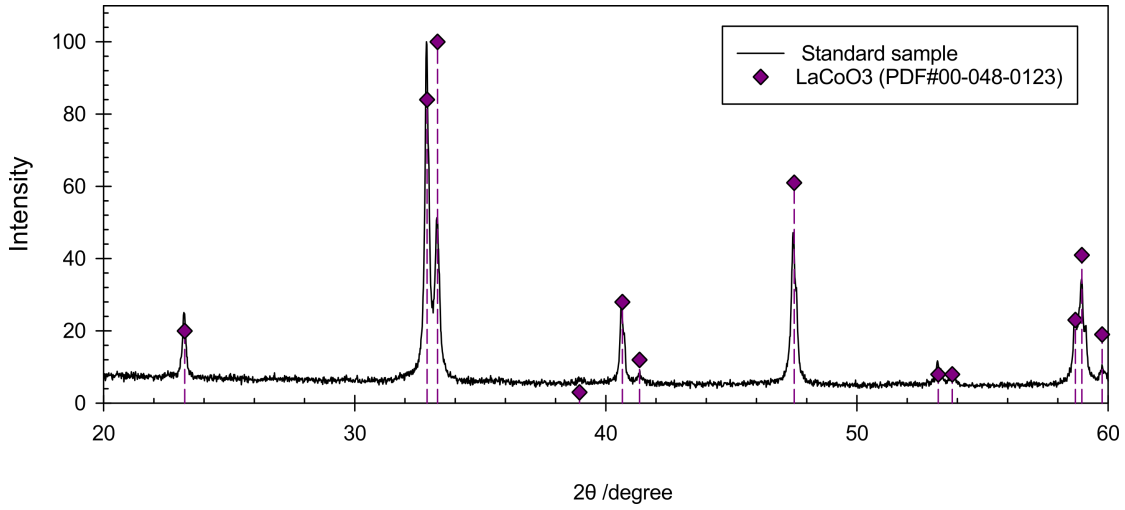

Figure 5.1: X-ray diffractogram of standard sample containing $LaCoO_3$.

With the standard sample, the EPMA-WDS was calibrated to reduce the systematic error of the measured La:Co ratio. To ensure correct calibration the La:Co ratio of the standard sample was measured using EPMA-WDS analysis with $LaCoO_3$ as a standard. The data points were arranged in a histogram presented in Figure 5.2, showing number of points versus the cationic fraction $\xi = n_{La}/(n_{La} + n_{Co})$. The histogram shows that the measured ratio scatters in the range around $\xi = 0.5$ and is not as precise as desired. The mean value with the expanded uncertainty was calculated to be 1.0045 ± 0.003.

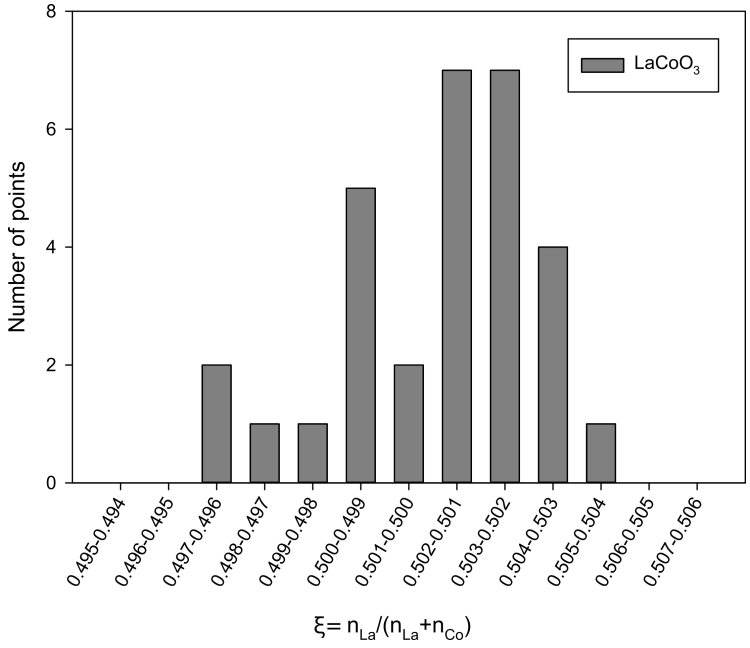

Figure 5.2: Histogram showing the number of data measured points in the standard sample of La_2CoO_4 versus the cationic fraction.

Using the measured La:Co of the standard sample, values measured later was corrected manually to achieve a more reliable result. The method of manually correcting the La:Co ratio is described in Appendix A.

5.2 Heat treatment at 900°C

Samples A2 and B2 were heat treated at 900°C at 120 hours in argon flow atmosphere with cobalt present. The sample compositions were characterised using XRD, and the X-ray diffractogram is presented in Figure 5.3. Both samples have peaks below the blue, red and green symbols indicating the presence of the phases La_2O_3, La_2CoO_4 and $La_4Co_3O_{10}$, respectively.

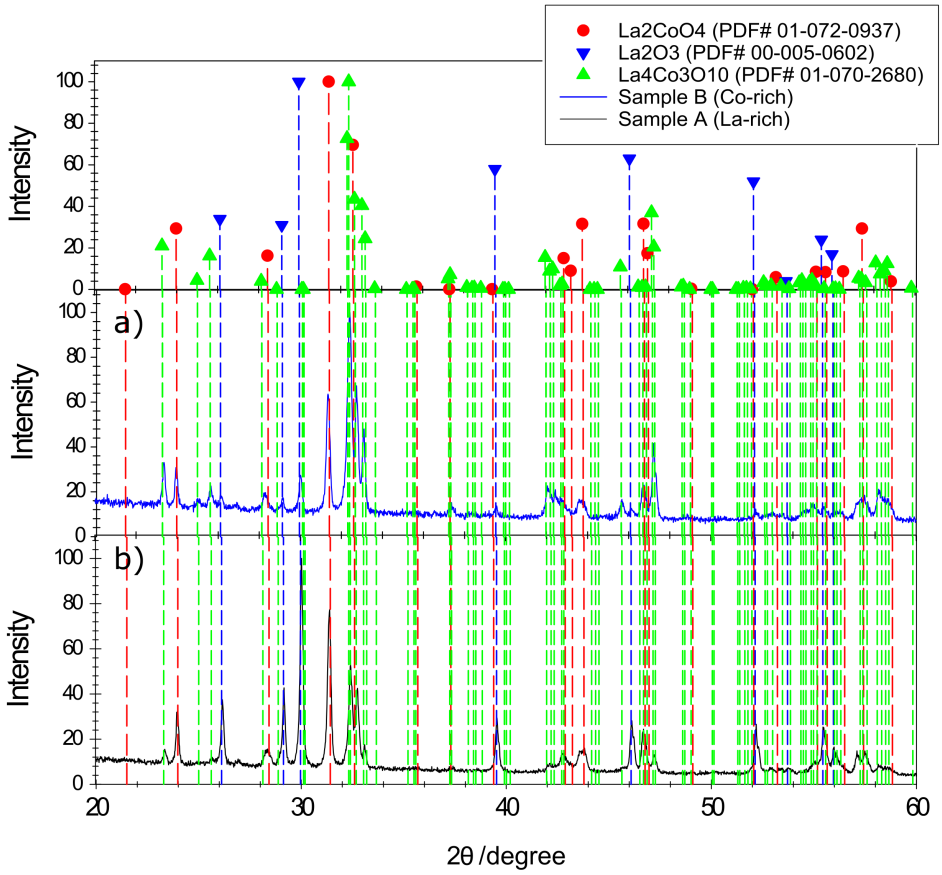

Figure 5.3: X-ray diffractograms of of samples A2 and B2 after heat treatment at 900°C for 120 hours in argon flow atmosphere and with cobalt present.

The samples were examined using EPMA to determine the average grain size. Backscattering images of the samples were taken with different magnifications shown in Figure 5.4 and Figure 5.5. The average grain size of samples A2 and B2 were determined from Figure 5.4b and 5.5b to be $0.571 \pm 0.048 \mu$m and $0.914 \pm 0.171 \mu$m, respectively.

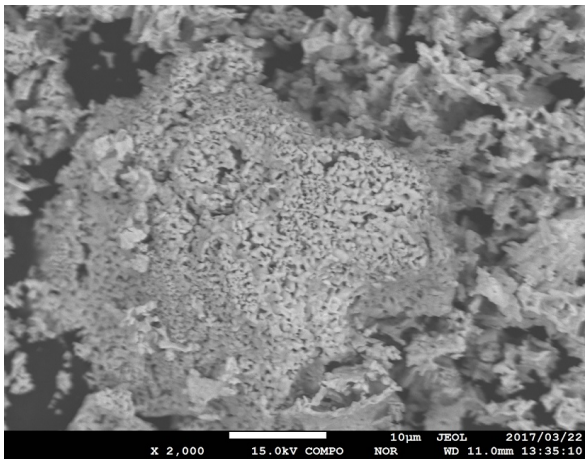

(a) Backscattering image of sample A2 at 2000X.

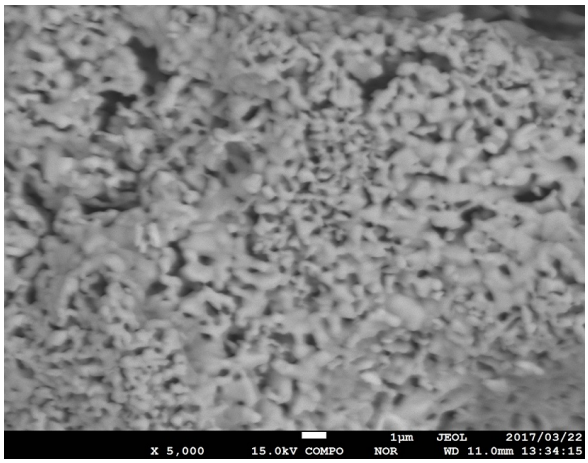

(b) Backscattering image of sample A2 at 5000X.

Figure 5.4: Backscattering images of sample A2.

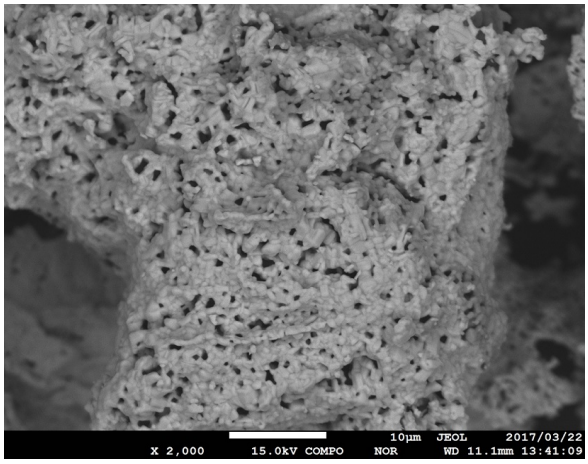

(a) Backscattering image of sample B2 at 2000X

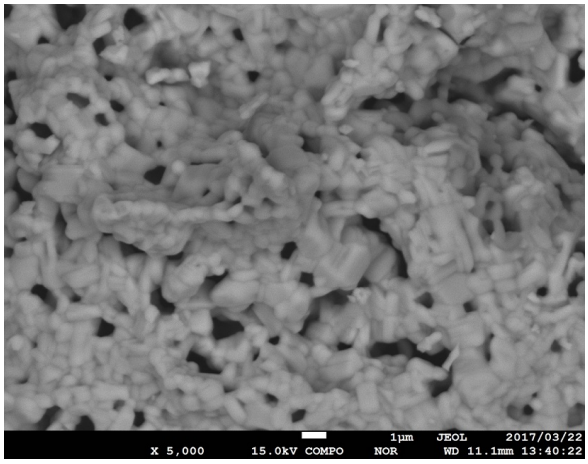

(b) Backscattering image of sample B2 at 5000X.

Figure 5.5: Backscattering images of sample B2.

The grain size of the samples was too small to use EPMA-WDS to determine the La:Co ratio of the La_2CoO_4 phases. TEM-EDS were used to try to determine the La:Co ratio. Figure 5.6 shows the mapping of Co and La in a particle from sample A2, which indicates that the particles contained both elements.

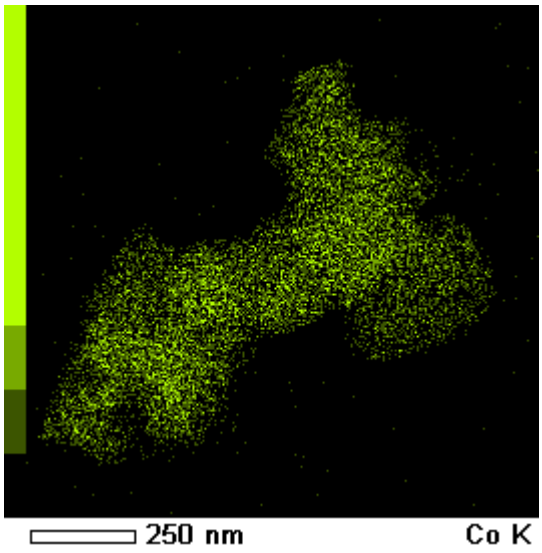

(a) Mapping of cobalt.

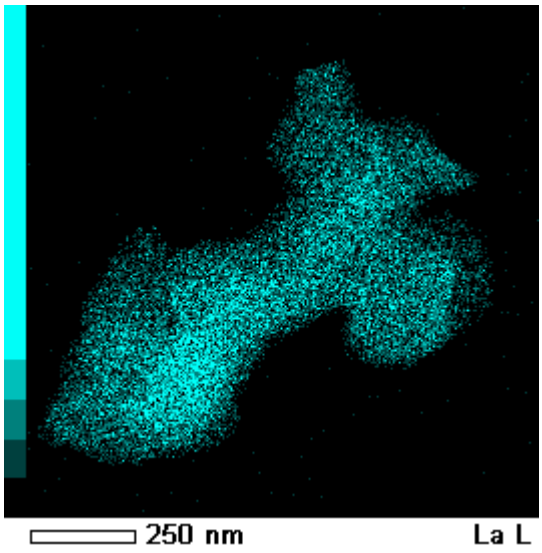

(b) Mapping of lanthanum.

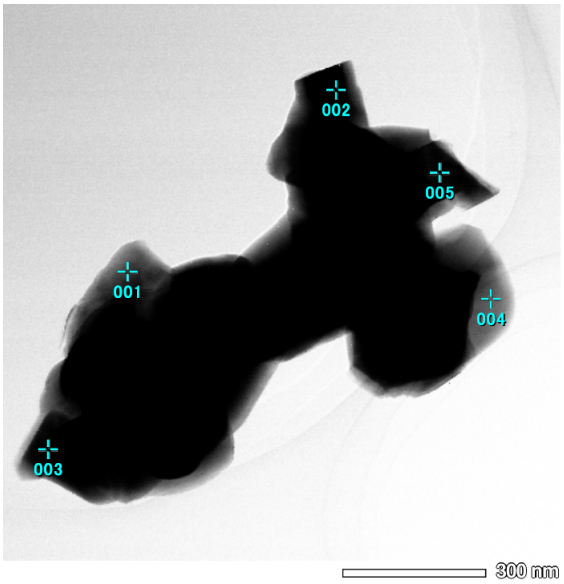

(c) Particle with points indicating where La and Co content were measured.

Figure 5.6: Mapping of Co (a) and La (b) in a particle in sample A2 taken with TEM.

The La:Co ratio of samples A2 and B2 were taken at several points of several particles as indicated in Figure 5.6c. Both samples had a high density of points around the cationic fraction, $\xi = 0.6$. The cationic fraction of the phases La_2CoO_4 and $La_4Co_3O_{10}$ lie in this area. A histogram is shown in Figure 5.7 and shows the number of points versus ξ around $\xi = 0.6$ to separate the two phases from each other.

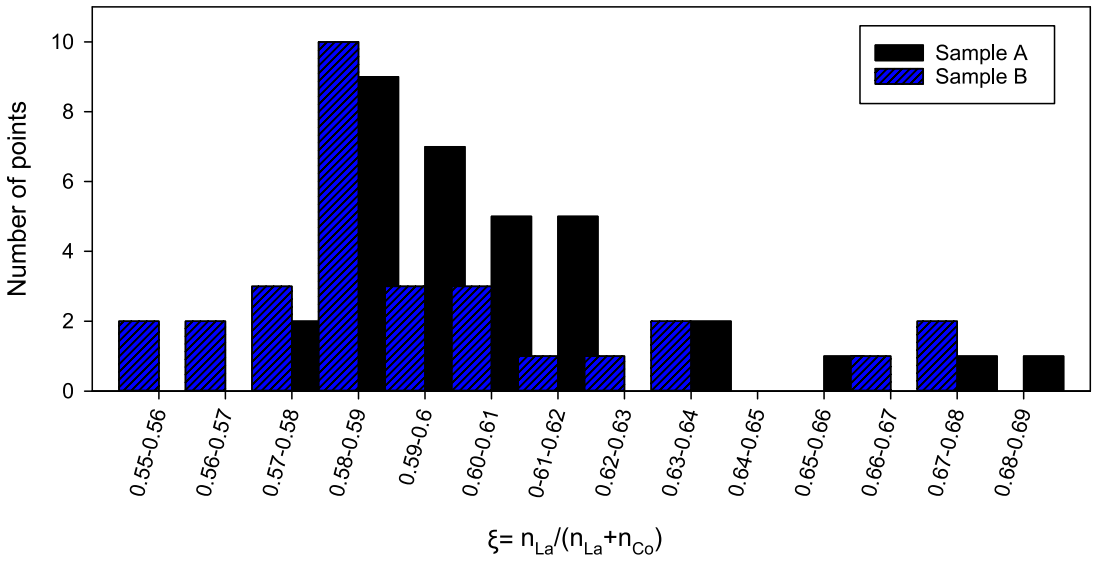

Figure 5.7: Histogram presenting the number of points versus the cationic fraction measured of samples A2 and B2. The cationic fraction was measured using TEM-EDS.

From the histogram, two phases can be seen in both sample A2 and B2. From the histogram one phase lies around $\xi = 0.59$ which is consistent with $La_4Co_3O_{10}$ ($\xi = 0.57$), while the one phase with a smaller set of measured points can be seen around $\xi = 0.67$ consistent with La_2CoO_4 ($\xi = 0.66$). However, from this result it is not possible to determine if the La_2CoO_4 has any stability range.

5.3 Heat treatment at 1100°C

Sample A1 and Sample B1 heat treated at 1100°C were characterised using XRD to identify the phases present. The X-ray diffractograms are presented in Figure 5.8. Sample A1 had peaks below the red and blue symbols, indicating a presence of La_2CoO_4 and La_2O_3, respectively, in the sample. The peaks in the diffraction pattern of sample B1 were directly below the red and green symbols indicating the presence of the phases La_2CoO_4 and $La_4Co_3O_{10}$, respectively.

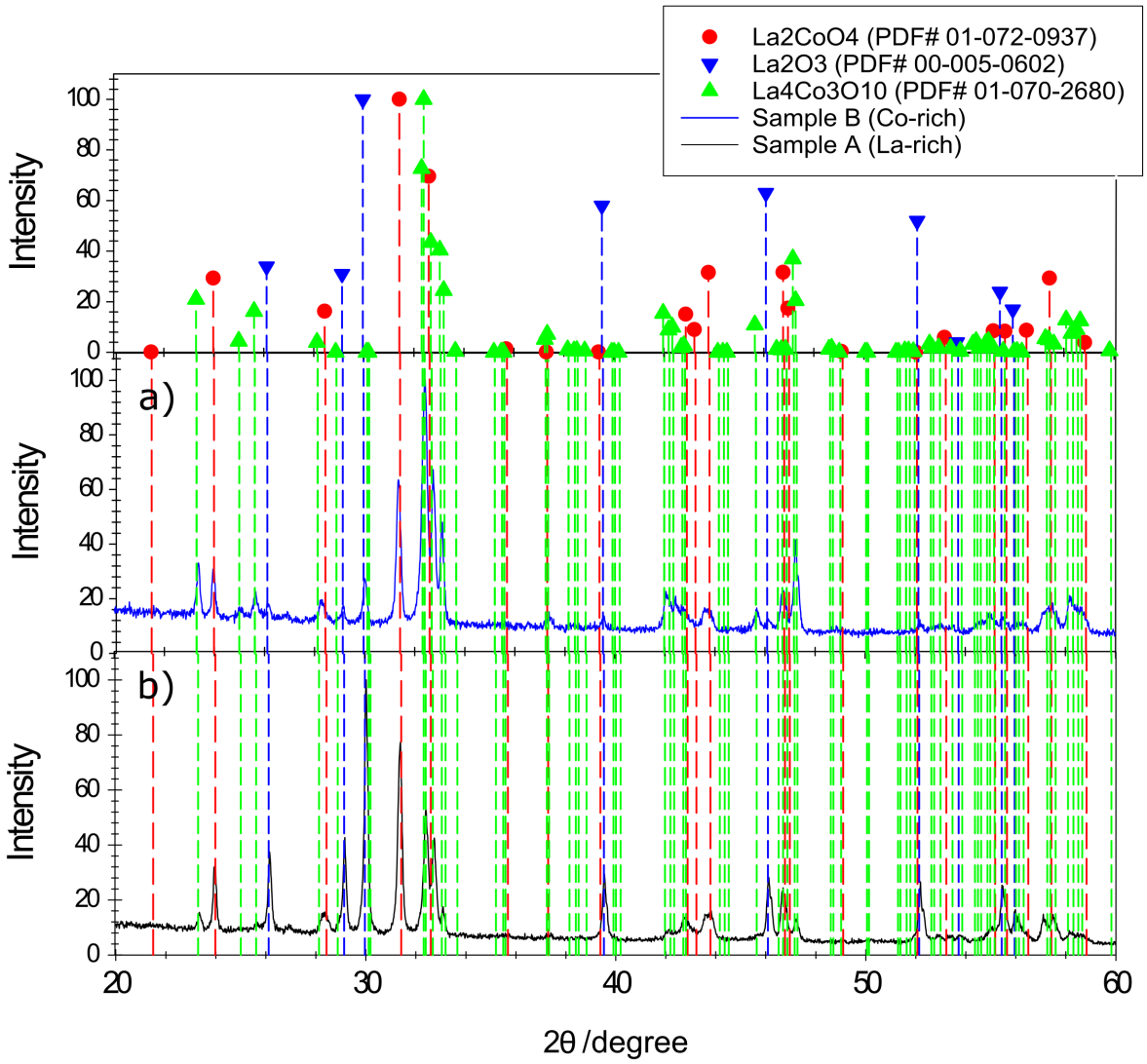

Figure 5.8: X-ray diffractograms of samples B1 (a) and A1 (b) after heat treatment at 1100°C for 10 hours.

Samples A1 and B1 were examined using EPMA to determine the grain size and backscattering images, shown in Figures 5.9 and 5.10, respectively, were taken. The average grain size of the samples was estimated from the images to be $1.729 \pm 0.257 \mu$m and $1.92 \pm 0.180 \mu$m.

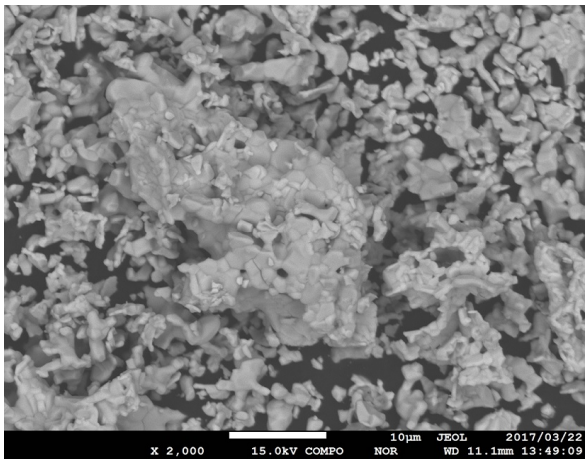

(a) Backscattering image of sample A1 at 2000X.

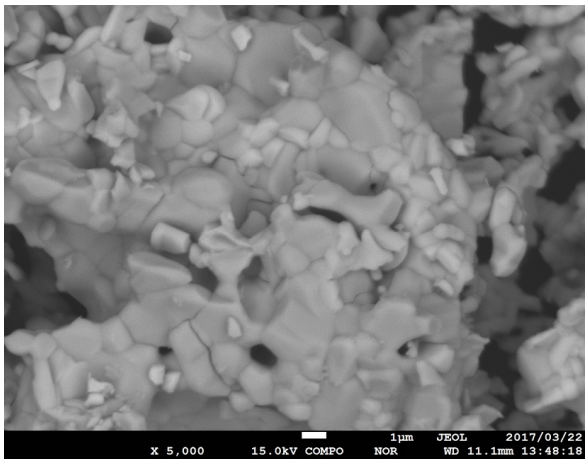

(b) Backscattering image of sample A1 at 5000X.

Figure 5.9: Back scattering images of sample A1.

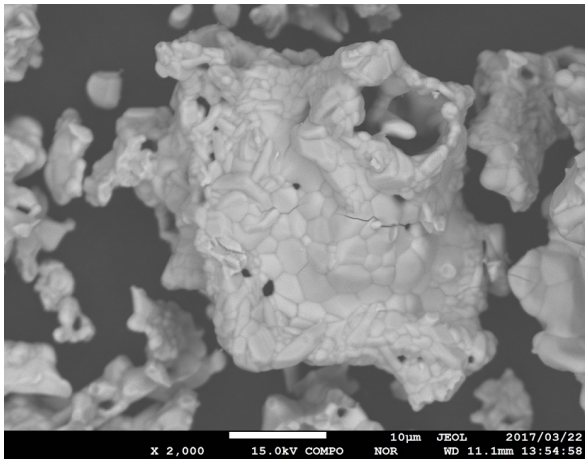

(a) Backscattering images of sample B1 at 2000X

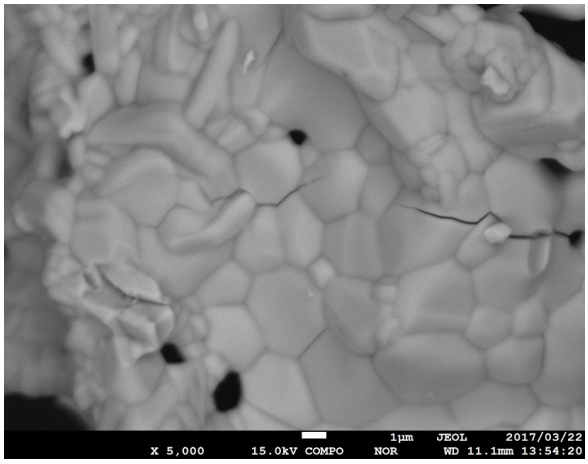

(b) Backscattering image of sample B1 at 5000X.

Figure 5.10: Back scattering image of sample B1.

From the images, the different phases could not be distinguished from each other. Using EPMA-WDS the La:Co ratio was measured. The La:Co ratio was measured in a 5X5 point grid on several particles. Figure 5.11 shows the measured points on a particle of sample A1.

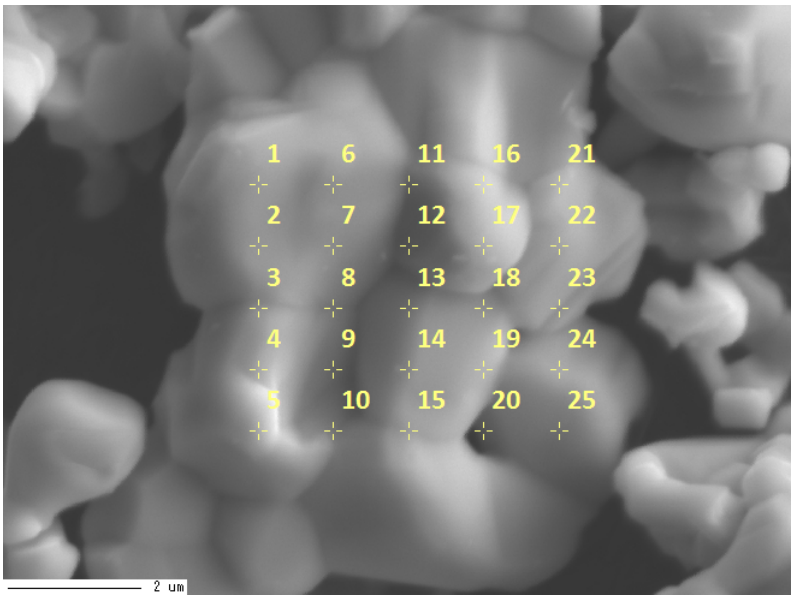

Figure 5.11: Secondary electron image of sample A1 with a 5X5 grid showing where La/Co ratio was measured.

Only points with a mass percent higher than 90% were included in the calculation of the average La/Co ratio of the La_2CoO_4 phase. Points who had a La/Co indicating another phase in the sample were excluded. Figure 5.12 shows a histogram of the number of points versus the cationic ratio, ξ.

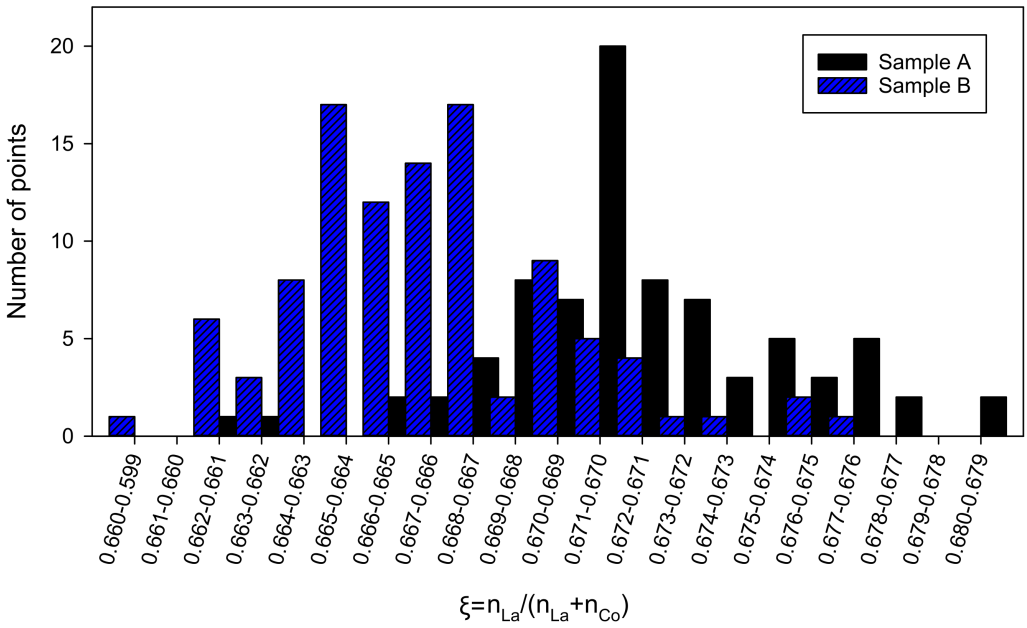

Figure 5.12: Histogram presenting the number of points versus the cationic fraction measured of samples A1 and B1.

The histogram shows that there is some deviation between the cationic fraction of samples A1 and B1. The measurements of sample B1 are on average lower in value compared to sample A1. The average La:Co ratio with the expanded uncertainty was found to be 2.0550 ± 0.0158 and 1.9997 ± 0.0056 for samples A1 and B1, respectively. The average cation ratio of both samples lies close to the stoichiometric value of 2, but the samples deviate slightly from each other.

5.3.1 Low-temperature oxidation

Samples A1 and B1 were heat treated at 600°C in air for 100 hours, and the product was examined by XRD analysis. The X-ray diffractograms of sample A1 before and after the heat treatment are shown in Figure 5.13.

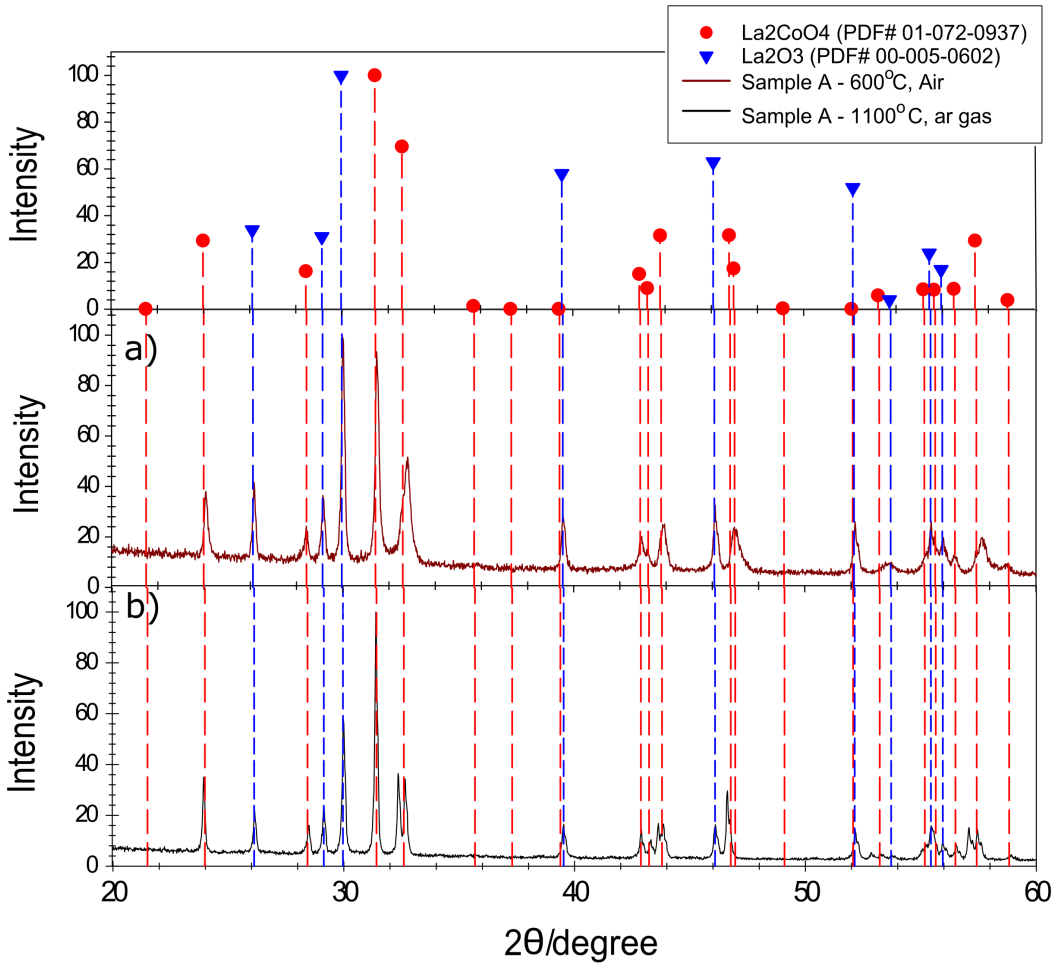

Figure 5.13: X-ray diffractograms sample A1 before (b) and after (a) oxidation at 600°C in air.

It can be seen that the phase composition does not change during the low-temperature heat treatment and sample A1 still have La_2CoO_4 and La_2O_3 phases present indicated by the peaks located directly below the red and blue symbols, respectively. An enlarged view of the diffraction pattern shown in Figure 5.14, shows some change in the diffraction peaks belonging to the La_2CoO_4 phase. The peaks at $2\theta = 32.5°$ and $2\theta = 43.6°$, indicated with black arrows in Figure 5.14, were separated after the initial heat treatment at 1100°C, but after the low-temperature heat treatment in air, the peaks are overlapping each other. The Miller indices related to the peaks show that the overlapping occurs because of change in the a and b lattice parameters.

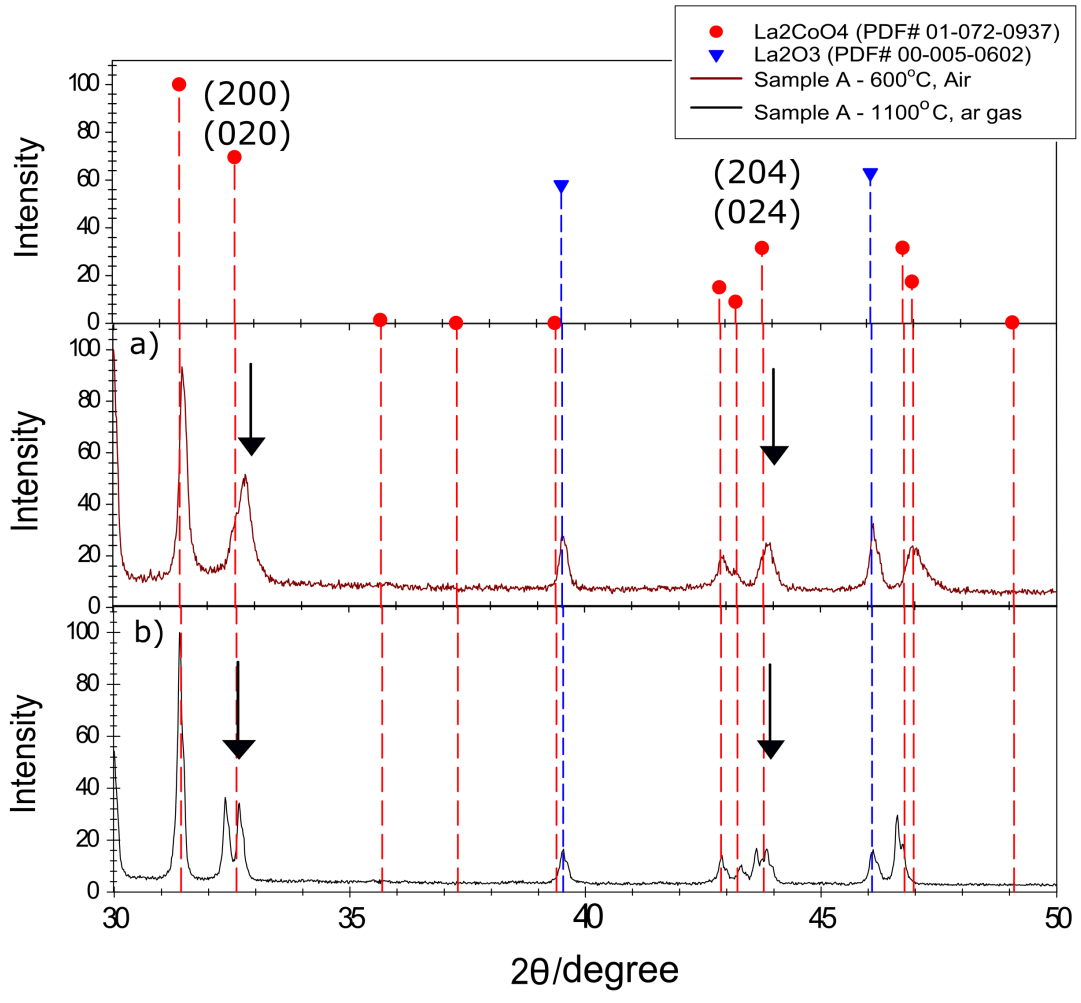

Figure 5.14: X-ray diffractograms of sample A1 before (b) and after (a) oxidation at 600°C in air. The arrows indicate where a change in the diffractograms is observed.

The X-ray diffractograms of sample B1 before and after low-temperature oxidation in air are shown in Figure 5.15. The diffraction pattern shows the presence of the same two phases;

La_2CoO_4 and $La_4Co_3O_{10}$ by the peaks located below the red and green symbols, respectively, indicating no change in the phase composition.

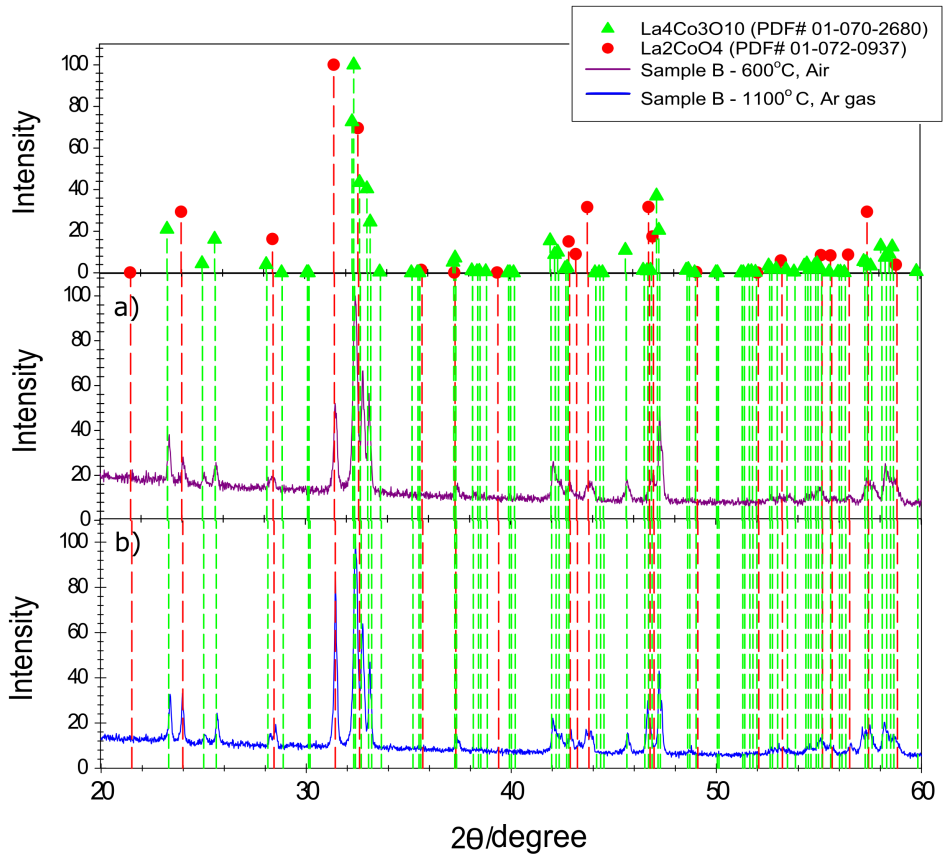

Figure 5.15: X-ray diffractograms of sample B1 before (b) and after (a) oxidation at 600°C in air.

An enlarged view, shown in Figure 5.16, of some areas of the diffraction patterns does show some changes to the peaks. A small change is seen at $2\theta = 44°$ indicated by a black arrow Figure 5.16, where the two peaks overlap more after the low-temperature oxidation than what they did before. The peaks are related to the Miller indices (024) and (204) with a variation in lattice parameter a and b.

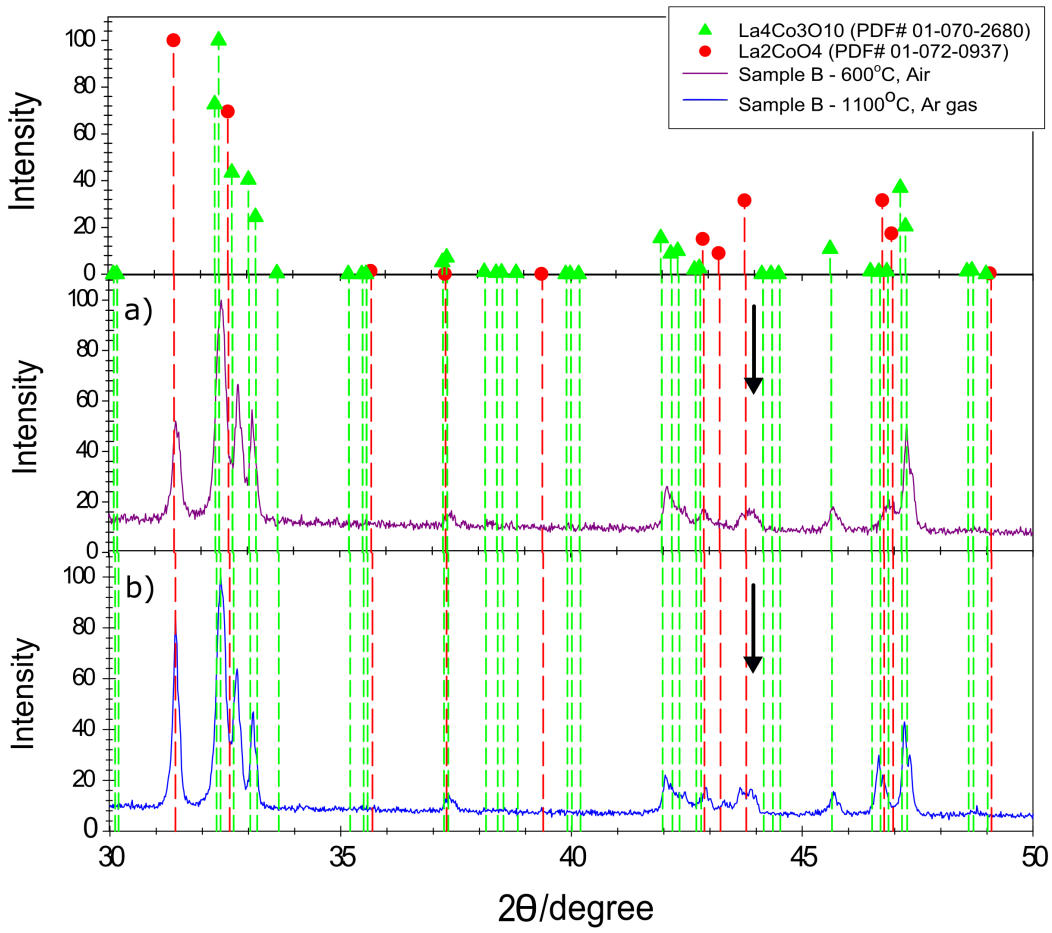

Figure 5.16: X-ray diffractograms of sample B1 before (b) and after (a) oxidation at 600°C in air. The arrow indicated where a change in the diffractogram was observed

5.3.2 Lattice parameters

The lattice parameters for samples A1 and B1 were found using Rietveld refinement and are presented in Table 5.1 below. The lattice parameters retrieved using Rietveld refinement were compared to manually calculated values to ensure the validity of the results. The manally calculated lattice parameters are presented in Tables B.2 and B.4 found in Appendix B.

Table 5.1: Calculated lattice parameters using Rietveld refinement. The number in the parentheses is the standard deviation on the last number.

Sample	**a [Å]**	**b [Å]**	**c [Å]**
A1	5.5312(2)	5.4829(1)	12.5368(3)
B1	5.5323(4)	5.4818(8)	12.5430(4)

The lattice parameters were found using Rietveld refinement for sample A1 and B1 after the low-temperature oxidation in air. The lattice parameters are shown in Table 5.2. The lattice parameters were compared to manually calculated values to ensure the validity of the results. The manually calculated lattice parameters are presented Tables B.6 and B.8 found in Appendix B.

Table 5.2: Calculated lattice parameters using Rietveld refinement. The number in the parentheses is the standard deviation on the last number.

Sample	**a [Å]**	**b [Å]**	**c [Å]**
A1 - 600°C	5.4887(5)	5.4557(5)	12.5738(11)
B1 - 600°C	5.5076(9)	5.4599(17)	12.5622(9)

In Figure 5.17 the change in the unit cell is presented as a function of the treatment condition. Parameter a and b decreases in both samples as the partial oxygen pressure is increased. The parameters, a and b of sample A1, have a higher decrease than that of B1. Parameter c increases as a function of the partial oxygen pressure. The same tendency can be found here, that parameter c for A1 has a higher increase in value. From this result, it can be seen that the lattice parameters of samples A1 and B1 were more similar before the low-temperature oxidation and had a more distinct difference in the parameter values after the treatment.

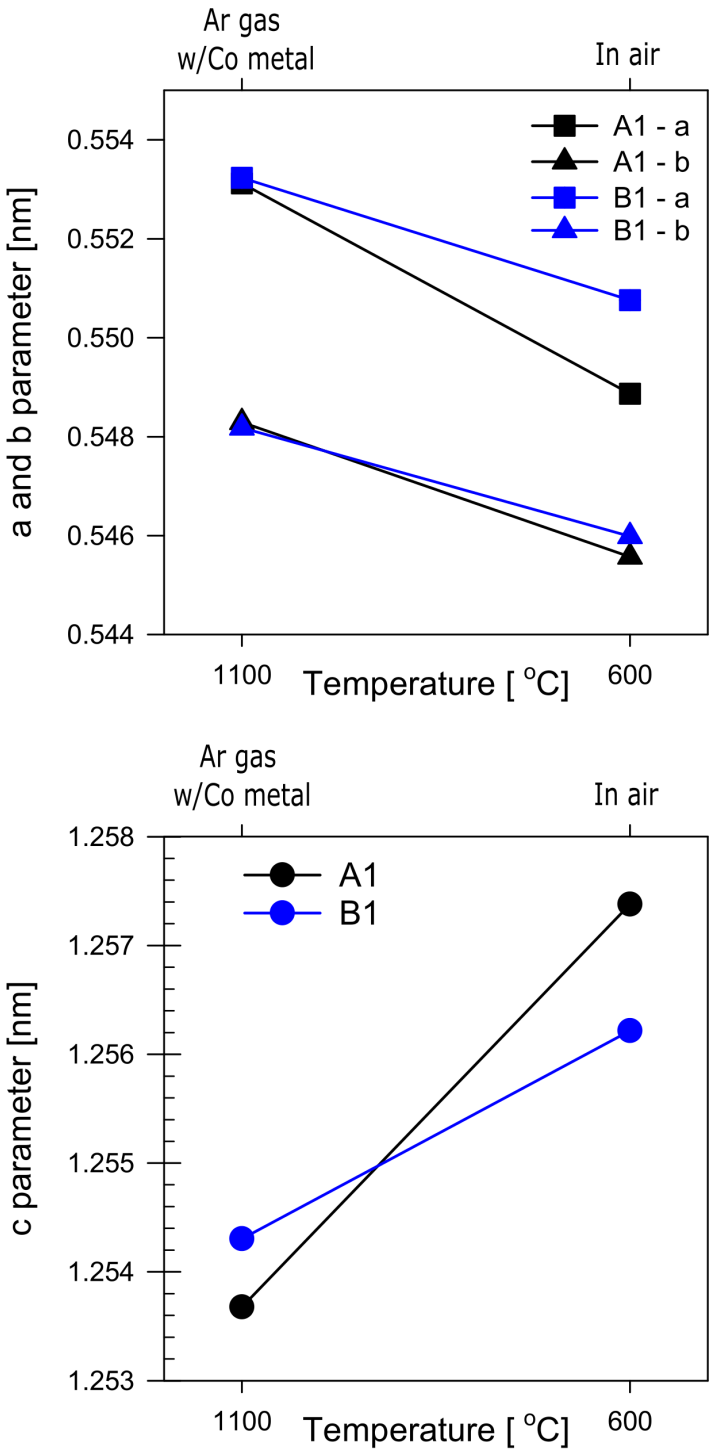

Figure 5.17: Parameters a and b (top) and c (bottom) as a function of the heat treatment conditions.

Chapter 6

Discussion

In this discussion, the results presented in Chapter 5 will be explained and understood based on earlier work in similar studies. Through this discussion it will be clarified if La_2CoO_4 contains any cation nonstoichiometry and if this result supports the existence of the lanthanum deficient $La_{1.83}CoO_{4-x}$ reported by Lewandowski *et al.* [7].

In this study only one sample of each La:Co ratio was prepared and studied, and should be taken into account when determining the reliability of the results which this discussion is based on. The average La/Co ratio was measured using several points to increase the likelihood of the value being reliable.

6.1 Heat treatment at 900°C

Two types of samples with different La:Co ratio of 75:25 and 60:40 were heat treated at 900 °C, named A2 and B2, respectively. The X-ray diffractograms presented in Figure 5.3 indicated the same three phase compositions in both samples consisting of La_2CoO_4, $La_4Co_3O_{10}$ and La_2O_3 after the heat treatment in 120 hours. From the isothermal (1273K) phase stability diagram shown in Figure 3.4 it can be seen that this three-phase composition is stable for both the La-rich and Co-rich samples only within a narrow oxygen partial pressure range. One reason that a three-phase composition was found in both samples is that p_{O_2} was in this narrow range for three-phase equilibrium. This would indicate that the oxygen absorption by Co metal was insufficient due to kinetic reasons. In this case, the composition of

La_2CoO_4 in samples A2 and B2 should be the same, and it would not be possible to analyse the composition range of La_2CoO_4.

Another possibility could be that the reactions within the samples were too slow to reach two-phase equilibrium during the heat treatment even though p_{O_2} was low enough. In this case, the composition of the La_2CoO_4 will vary from position to position in the samples. This explanation seems likely in this case since the grain sizes in samples A2 and B2 determined by backscattering images shown in Figures 5.4 and 5.5, were small and the samples did not seem to be fully equilibrated. It would be possible to analyse the composition range of the of the La_2CoO_4 phase with a very accurate TEM-EDS. However, this is difficult in practice because of measurement errors.

The samples were analysed using TEM-EDS to measure the La:Co ratio of the La_2CoO_4-phase to determine if any lanthanum deficient phases exist. Figure 5.7 show the measured data from the analysis. From the measured data it is hard to verify if any cation nonstoichiometric La_2CoO_4 phases are present in the samples. Both samples have a peak close to $\xi = 0.59$ which is consistent with the $La_4Co_3O_{10}$ phase which earlier XRD analysis confirmed the presence of in the samples. The majority of the points measured seem to come from this phase. There are also several points measured with a higher cationic fraction of $\xi = 0.67$ which indicate the presence of the stoichiometric La_2CoO_4 phase. However, the data suggest that only a small amount of points was measured of the La_2CoO_4, making it hard to say with high confidence that these points are of the stoichiometric phase. Both the cation nonstoichiometric phase suggested by Lewandowski *et al.* [7] and the stoichiometric phase have a cationic fraction value shown in Equations 6.1 and 6.2, which lie within the experimental results.

$$La_{1.83}CoO_4 : \frac{La}{La + Co} = 0.647 \tag{6.1}$$

$$La_2CoO_4 : \frac{La}{La + Co} = 0.667 \tag{6.2}$$

The proximity between the cationic fraction of the two phases and the data obtained from TEM-EDS makes it hard to say anything about the cation stoichiometry of the compound in these samples, and it is hard to judge if the La_2CoO_4 phase has any composition range. From the histogram in Figure 5.7 one can also see a broad distribution of bars between the composition of $La_4Co_3O_{10}$ and La_2CoO_4. This suggests that even though only single points of a particle were analysed using TEM-EDS, signals from both compositions were detected. Some systematic error in the equipment could also have led to the data measured deviating from the real number.

The data collected from heat treatment at 900°C gave no result which could be used to determine if a cation nonstoichiometric La_2CoO_4 phase exists or if the phase has any stability range. Therefore, it was decided to focus most of the experimental work performed in this study on the samples heat treated at 1100°C due to them being better equilibrated and having a larger grain size.

6.2 Heat treatment at 1100°C

Figure 5.8 shows the X-ray diffractograms of samples A1 and B1 after heat treatment at 1100°C for 10 hours. Sample A1 has a two-phase composition of La_2CoO_4 and La_2O_3 which is expected for the La:CO ratio 75:25 from the phase stability diagram shown in Figure 3.4. Sample B2 with a La:Co ratio of 60:40 also had an expected two-phase composition consisting of La_2CoO_4 and $La_4Co_3O_{10}$. The isothermal phase diagram for 1100°C deviate slightly from the isothermal phase stability diagram for 1273K shown in Figure 3.4, but using the desired phases was achieved based on this diagram nonetheless. The grain sizes were found to be large enough so the La:Co ratio of the La_2CoO_4-phase could be determined using EPMA-WDS ($> 1\mu$m).

The average cation ratio in the samples was determined to be equal to 2.0550 ± 0.0158 and 1.9997 ± 0.0056 for samples A1 and B1, respectively, using EPMA-WDS. The La:Co ratio was measured with a $LaCoO_3$ as a standard sample to eliminate any systematic error. Using the data from the standard sample the numbers were then corrected manually, since the measurements of the standard sample shown in Figure 5.2 did scatter. The obtained cation ratio lies close to the stoichiometric value equal to two. Since the data have been corrected for any

systematic error and the average cation ratio is measured from several points in the samples, the obtained ratio should be close to the real value. This result is supported by the work performed by Seppänen *et al.* and Kitayama [6, 9, 10].

The values average cation ratio of the samples deviate from each other slightly. The difference in the values can also be seen in the histogram presented in Figure 5.12. This difference indicates that the La_2CoO_4-phase might have some composition range as a function of the La:Co ratio which lies close to the stoichiometric La:Co value equal to two. However, the difference between the average cation ratio of samples A1 and B1 is small. Based on the results reported by Lewandowski *et al.* [7] a larger difference would be seen between the measured values, so the results from this work does not support the suggested formula of $La_{1.83}CoO_{4-x}$.

6.2.1 Low-temperature oxidation in air

After being heat-treated at 1100°C under a low oxygen partial pressure, samples A1 and B1 went through a low-temperature oxidation in air at 600°C for 100 hours. In their work Lewandowski *et al.* [7] performed a low-temperature oxidation which resulted in samples containing a fully oxidised La_2CoO_4-type phase and secondary phases depending on the La:Co ratio of the samples. The work was briefly presented in Chapter 2, and Figure 2.1 shows the results of their low-temperature oxidation experiment.

Figure 5.13 and 5.15 show the X-ray diffractograms before and after the low-temperature oxidation for samples A1 and B1, respectively. The phases in the samples did not change during the low-temperature oxidation. This deviates from the results presented by Lewandowski *et al.* [7] where the low-temperature oxidation resulted in variation in phase composition depending on the La/Co ratio of the samples. If the stoichiometric La_2CoO_4 phase is unstable and La-deficient La_2CoO_4 is stable after low-temperature oxidation, it would be expected to see results indicative of this. One possible outcome is that the La_2CoO_4 decomposes to a La-deficient La_2CoO_4 phase with a secondary phase such as La_2O_3, which would be detected by analysis using XRD. Another possible result is that a La-deficient La_2CoO_4 phase is formed by diffusion of Co from the $La_4Co_3O_{10}$ phase to the La_2CoO_4 phase in sample B1 represented by the following equation:

$$a\mathrm{La_2CoO_4} + b\mathrm{La_4Co_3O_{10}} = a'\mathrm{La_{2-x}CoO_4} + b'\mathrm{La_4Co_4O_{10}} \tag{6.3}$$

For this reaction to occur the Co atoms must move over a long distance at this temperature. Because of this, this case seems unlikely but should not be fully neglected.

From the low-temperature oxidation performed in this work, the results showed no indication of a La deficiency La_2CoO_4 phase. It should be noted that the La_2CoO_4 phase is not thermodynamically stable at 600°C in air since p_{O_2} will be too high, and therefore will La_2CoO_4, in the end, decompose regardless of the La/Co ratio. Because of this low-temperature oxidation is not an ideal method to be used to investigate the composition range of La_2CoO_4.

An enlarged view of the X-ray diffractograms shown in Figures 5.14 and 5.16 makes it possible to observe that there is some change in the peak position of peaks related to the La_2CoO_4 phase. Several distinct peaks that were separated before the low-temperature oxidation shifted into a more overlapping position. The Miller indices for these peaks show that the change is due to a change in the a and b parameters of these planes. The change in peak position is most likely due to oxidation, as oxygen will occupy interstitial sites. Comparing the X-ray diffraction pattern presented in the paper by Ram *et al.* [8] the same tendency can be found with the peaks overlapping more as the excess oxygen increases.

In their studies Lewandowski *et al.* [7] the products after the low-temperature oxidation were analysed using XRF and the result was compared with the XRD result. This is shown in Table 2.1. Together, these measurements indicated a La/Co ratio close to 1.85 and that the compound was lanthanum deficient. Thermogravimetry and titration were also performed as part of the work which indicated nonstoichiometry in the compound, but these methods do not distinguish between La deficiency and oxygen excess. Since the work in this study along with earlier work performed by others [6, 9, 10] do not support this result, a possible explanation could be that the XRF measurements performed were not correct.

6.2.2 Lattice parameters

The lattice parameters of La_2CoO_4 in samples A1 and B1 after the initial heat treatment at 1100°C were calculated and presented in Table 5.1. The lattice parameters lie close in value and does not indicate any substantial structural difference between the two samples. Both samples have a very similar value of parameters a and b. There is a large difference in the value of parameter c, but the deviation between the samples is small. When comparing the values found in this work to the lattice parameters reported by Lewandowski *et. al* [7] of the lanthanum deficient compounds, they seem to lie very close in value, but it is hard to see any clear relation between the values. By comparing the values to other literature values reported in several other papers of La_2CoO_{4+x} they fit into the reported range but do not show any clear correlation to a specific phase reported [8, 20, 33].

After the low-temperature oxidation, the unit cell parameters of the La_2CoO_4-phase in samples A1 and B2 were found using Rietveld refinement which is presented in Table 5.2. Comparing these values to the lattice parameters reported in other literature values no direct correlation between any specific values can be seen, but they fit into the reported range which is similar to the values discussed in the last paragraph.

Figure 5.17 shows the change in lattice parameters in samples A1 and B1 after the low-temperature oxidation. Both samples show the same trend where a and b are reduced, and parameter c is extended as the compound is oxidised. The elongation parallel to the c axis has been reported earlier by other authors [34]. This elongation can be explained by the extra oxygen ions, which occupy the interstitial positions on the rock salt (AO) layer of the crystal structure. The same tendency can be seen for the similary structured La_2NiO_4 where the excess oxygen content, δ, is increasing with increasing value of 2c/(a+b) [35]. However, some papers report that La_2CoO_4 shows the opposite effect compared to La_2NiO_4, meaning that a shortening of the c-axis is shown [20, 33]. Both La_2CoO_4 and La_2NiO_4 have shown to have a very high capability to take up excess oxygen, which makes it hard to obtain the stoichiometric phases [36]. Only under high-quality inert gases it is possible to synthesise the stoichiometric phases of these compounds.

6.3 Further work

In future work, it could be interesting to continue investigating the composition range of the La_2CoO_4 phase at 900°C, since the work from this study did not give any result of which a conclusion could be drawn at this temperature. From the data obtained from the analysis and characterisation of La_2CoO_4 after heat treatment at 1100°C, and from previous studies, the results support that there is little to no cation nonstoichiometry in this compound. Therefore, there might not be necessary to continue investigating if the compound has any significant La deficiency.

The results of this work however indicate that some composition range could exist, though very small. Further work on La/Co ratios closer to the stoichiometric value could be interesting to determine this composition range in further detail.

It would be interesting to investigate the change in lattice parameters as a function of oxygen content in the La_2CoO_4, especially the elongation of the c-axis, since the results in this study could not be supported by the literature.

Chapter 7

Conclusion

The cation nonstoichiometry of La_2COO_4 and the composition range of the compound were studied in one La-rich sample and a Co-rich sample at two temperatures; 900°C and 1100°C. The studies were performed by analysis and characterization using XRD, EPMA-WDS and TEM-EDS. The results were compared to the work of Lewandowski *et al.* [7] which indicated that the compound was lanthanum deficient and suggested the formula $La_{1.83}CoO_{4-x}$.

Heat treatment of the La-rich (La:Co = 75:25) and Co-rich (La:Co = 60:40) at 1100°C resulted in a two-phase composition with a La_2CoO_4 phase with the measured La/Co ratio of 2.0550 ± 0.0158 and 1.997 ± 0.0056, respectively, indicating that the cation ratio is close to the stoichiometric value. Some cation nonstoichiometry might exist, but the composition range will be small.

A low-temperature oxidation of these samples resulted in no change in phase composition, but the lattice parameters describing the La_2CoO_4 phase changed. This change is consistent of oxidation leading to an excess of oxygen seen in similar studies, giving the formula $La_2CoO_{4+\delta}$.

Heat treatment of the La-rich and Co-rich samples at 900°C resulted in a three phase composition containing a La_2CoO_4. However, due to a slow reaction the samples were not equilibrated and consisted of small grains which made it difficult to draw any conclusions from the data collected.

Bibliography

[1] E. Baran, "Structural chemistry and physicochemical properties of perovskite-like materials," *Catalysis today*, vol. 8, no. 2, pp. 133–151, 1990.

[2] T. Ishihara, *Perovskite oxide for solid oxide fuel cells*. Springer Science & Business Media, 2009.

[3] S. C. Singhal, "Solid oxide fuel cells," *The Electrochemical Society Interface*, vol. 16, no. 4, p. 41, 2007.

[4] K.-D. Kreuer, *Fuel cells: selected entries from the encyclopedia of sustainability science and technology*. Springer Science & Business Media, 2012.

[5] O. T. Sørensen, "Studies of non-stoichiometric oxides by thermoanalytical methods," *Thermochimica Acta*, vol. 15, no. 2, pp. 227–237, 1976.

[6] M. Seppanen, M. Kyto, and P. Taskinen, "Stability of the ternary phases in the La–Co–O system," *Scandinavian Journal of Metallurgy*, vol. 8, no. 5, pp. 199–204, 1979.

[7] J. T. Lewandowski, R. A. Beyerlein, J. M. Longo, and R. A. McCAULEY, "Nonstoichiometric K_2NiF_4-type phases in the lanthanum-cobalt-oxygen system," *Journal of the American Ceramic Society*, vol. 69, no. 9, pp. 699–703, 1986.

[8] R. M. Ram, P. Ganguly, C. Rao, and J. Honig, "Preparation and characterization of $La_2CoO_{4+\delta}$," *Materials research bulletin*, vol. 23, no. 4, pp. 501–506, 1988.

[9] K. Kitayama, "Thermogravimetric study of the Ln_2O_3-Co-Co_2O_3 system," *Journal of Solid State Chemistry*, vol. 131, no. 1, pp. 18–23, 1997.

[10] K. Kitayama, "Thermogravimetric study of the Ln_2O_3-Co-Co_2O_3 system: I. Ln= La," *Journal of Solid State Chemistry*, vol. 73, no. 2, pp. 381–387, 1988.

[11] G. Hoogers, *Fuel cell technology handbook*. CRC press, 2002.

[12] X. Zhou and S. Singhal, "Fuel cells – solid oxide fuel cells | overview," in *in Encyclopedia of Electrochemical Power Sources* (G. E. inChief: Jürgen, ed.), pp. 1–16, Amsterdam: Elsevier, 2009.

[13] N. H. Behling, *Fuel cells: current technology challenges and future research needs*. Newnes, 2012.

[14] E. D. Wachsman and K. T. Lee, "Lowering the temperature of solid oxide fuel cells," *Science*, vol. 334, no. 6058, pp. 935–939, 2011.

[15] R. M. Ormerod, "Solid oxide fuel cells," *Chemical Society Reviews*, vol. 32, no. 1, pp. 17–28, 2003.

[16] R. Sayers, J. Liu, B. Rustumji, and S. Skinner, "Novel K_2NiF_4-type materials for solid oxide fuel cells: Compatibility with electrolytes in the intermediate temperature range," *Fuel Cells*, vol. 8, no. 5, pp. 338–343, 2008.

[17] A. Chroneos, B. Yildiz, A. Tarancón, D. Parfitt, and J. A. Kilner, "Oxygen diffusion in solid oxide fuel cell cathode and electrolyte materials: mechanistic insights from atomistic simulations," *Energy & Environmental Science*, vol. 4, no. 8, pp. 2774–2789, 2011.

[18] A. Kushima, D. Parfitt, A. Chroneos, B. Yildiz, J. A. Kilner, and R. W. Grimes, "Interstitialcy diffusion of oxygen in tetragonal la 2 coo 4+ δ," *Physical Chemistry Chemical Physics*, vol. 13, no. 6, pp. 2242–2249, 2011.

[19] P. Atkins, *Shriver and Atkins' inorganic chemistry*. Oxford University Press, USA, 2010.

[20] L. Le Dreau, C. Prestipino, O. Hernandez, J. Schefer, G. Vaughan, S. Paofai, J. M. Perez-Mato, S. Hosoya, and W. Paulus, "Structural modulation and phase transitions in $La_2CoO_{4.14}$ investigated by synchrotron x-ray and neutron single-crystal diffraction," *Inorganic chemistry*, vol. 51, no. 18, pp. 9789–9798, 2012.

[21] S. Ruddlesden and P. Popper, "New compounds of the K_2NiF_4 type," *Acta Crystallographica*, vol. 10, no. 8, pp. 538–539, 1957.

[22] S. Ruddlesden and P. Popper, "The compound $Sr_3Ti_2O_7$ and its structure," *Acta Crystallographica*, vol. 11, no. 1, pp. 54–55, 1958.

[23] D. E. Sands, *Introduction to Crystallography*. Dover Publications, 1975.

[24] Y. Adachi, N. Hatada, and T. Uda, "Sintering, electrical conductivity, oxygen non-stoichiometry, thermal expansion and thermal stability of ruddlesden-popper type cobaltite $La_4Co_3O_{10}$," *Journal of The Electrochemical Society*, vol. 163, no. 9, pp. F1084–F1090, 2016.

[25] A. Petrov, V. Cherepanov, A. Y. Zuyev, and V. Zhukovsky, "Thermodynamic stability of ternary oxides in Ln-Mn-O (Ln= La, Pr, Nd; M= Co, Ni, Cu) systems," *Journal of Solid State Chemistry*, vol. 77, no. 1, pp. 1–14, 1988.

[26] A. Petrov, V. Cherepanov, and A. Y. Zuev, "Thermodynamics, defect structure, and charge transfer in doped lanthanum cobaltites: an overview," *Journal of Solid State Electrochemistry*, vol. 10, no. 8, pp. 517–537, 2006.

[27] A. R. West, *Solid state chemistry and its applications*. John Wiley & Sons, 3 ed., 2014.

[28] P. J. Gellings and H. Bouwmeester, *Handbook of solid state electrochemistry*. CRC press, 1997.

[29] N. N. Greenwood and A. Earnshaw, *Chemistry of the Elements*. Elsevier, 2012.

[30] L. E. Smart and E. A. Moore, *Solid state chemistry: an introduction*. 4 ed., 2012.

[31] Callister and D. G. Rethwisch, *Materials science and engineering: An introduction*. John Wiley & Sons NY, 7 ed., 2007.

[32] G. Simkovich, *Transport in nonstoichiometric compounds*, vol. 129. Springer Science & Business Media, 2012.

[33] F. Girgsdies and R. Schöllhorn, "Spontaneous topotactic oxidation of La_2CoO_4 at room temperature," *Solid state communications*, vol. 91, no. 2, pp. 111–112, 1994.

[34] A. Aguadero, J. A. Alonso, and L. Daza, "Oxygen excess in $La_2CoO_{4+\delta}$: A neutron diffraction study," *Zeitschrift für Naturforschung B*, vol. 63, no. 6, pp. 615–622, 2008.

[35] M. Hücker, K. Chung, M. Chand, T. Vogt, J. Tranquada, and D. Buttrey, "Oxygen and strontium codoping of La_2NiO_4: Room-temperature phase diagrams," *Physical Review B*, vol. 70, no. 6, p. 064105, 2004.

[36] W. Paulus, A. Cousson, G. Dhalenne, J. Berthon, A. Revcolevschi, S. Hosoya, W. Treutmann, G. Heger, and R. Le Toquin, "Neutron diffraction studies of stoichiometric and oxygen intercalated La_2NiO_4 single crystals," *Solid State Sciences,* vol. 4, no. 5, pp. 565–573, 2002.

Appendix A

Correction of EPMA data

The concentration of elements in a sample is measured in WDS analysis by the strength of the X-ray signal the element gives out. The devices convert the signal to the concentration by the linear relationship shown in Figure A.1. In an ideal situation with a well-calibrated device, the measured concentration will be equal to the true concentration.

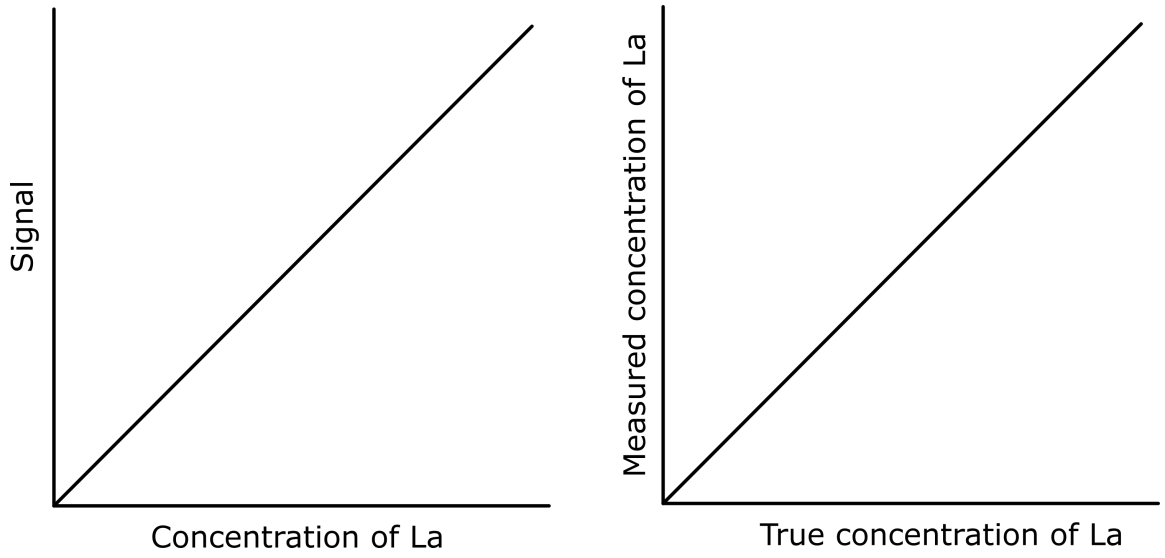

Figure A.1: (left) Signal vs. concentration of La and (right) measured concentration of La vs. true concentration of La in a ideal situation.

In reality, the relationship is often multiplied by a factor k, which make the measured data deviate from the true value. To correct the measured data to obtained the true value, k can be determined from a samples with a known concentration or ratio. The factor $\frac{k_{La}}{k_{Co}}$ can be found for $LaCoO_3$ assuming the La:Co ratio, $(\frac{x_{La}^{true}}{x_{Co}^{true}})$, is equal to 1 using the Equation A.1.

$$(\frac{x_{La}^{meas}}{x_{Co}^{meas}}) = (\frac{k_{La}}{k_{Co}})(\frac{x_{La}^{true}}{x_{Co}^{true}}) \tag{A.1}$$

Since the factor $\frac{k_{La}}{k_{Co}}$ is a universal factor it can be used to calculate the true La:Co ratio for La_2CoO_4 from the measured ratio. Using the measured cation ratio of the standard samples the universal factor was calculated to be $\frac{k_{La}}{k_{Co}} = 1.0045$.

Appendix B

Manual calculation of lattice parameters

The lattice parameters were found for samples A1 and B1 before and after low-temperature oxidation using Rietfield refinement. The same lattice parameters were calculated manually to confirm that the data is consistent.

The lattice parameters were calculated using the least square method and are given in Tables B.2, B.6, B.4,B.8 for sample A1 before and after low-temperature oxidation, and sample B1 before and after low-temperature oxidation, respectively.

B.1 Sample A1 heat treated at 1100°C

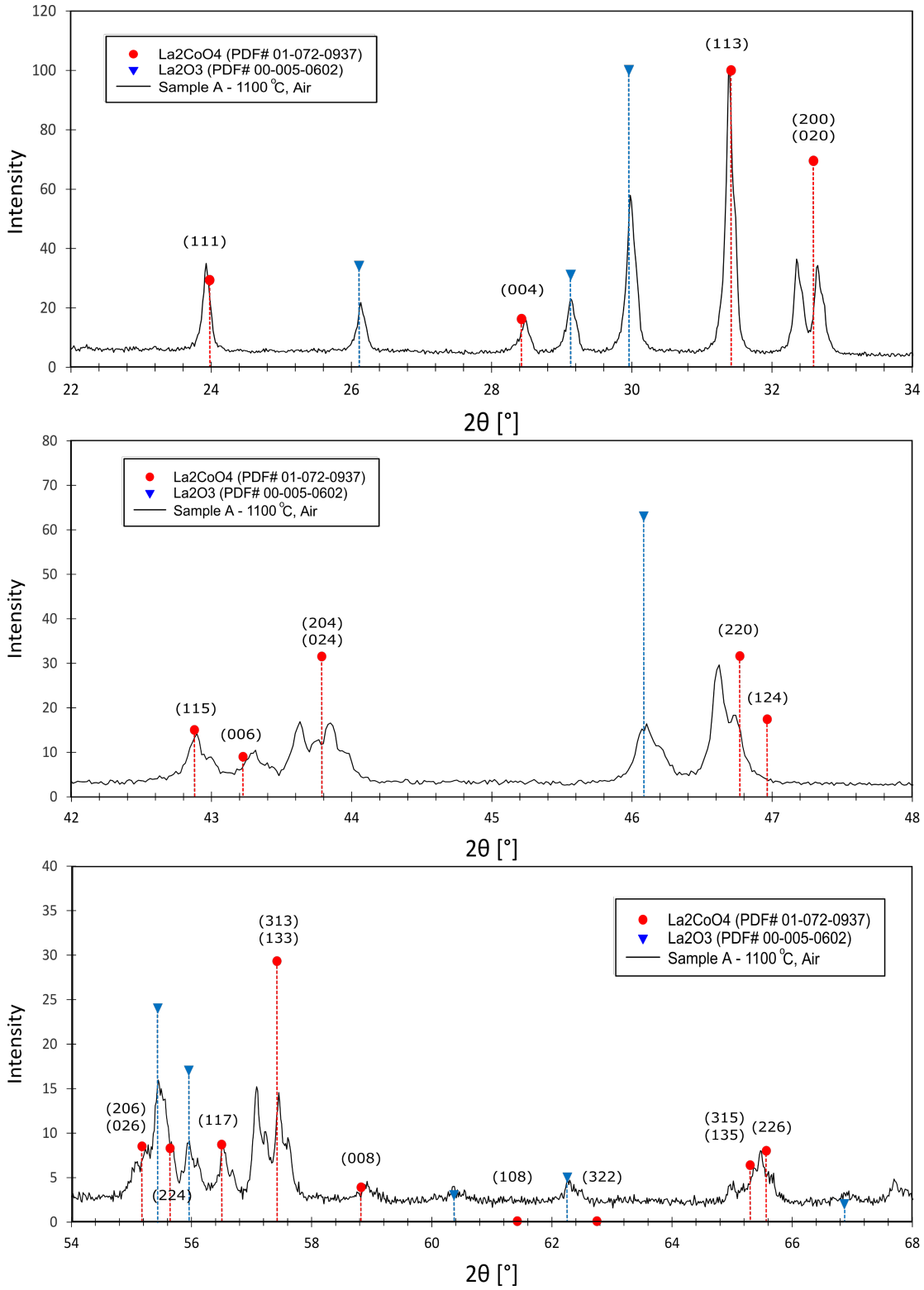

Figure B.1: Enlarged view of X-ray diffractogram of sample A1 in specific ranges; (top) $2\theta = 22 - 34°$ (middle) $2\theta = 42 - 48°$ (bottom) $2\theta = 54 - 68°$.

Table B.1: Position of peak related to the La_2CoO_4 phase, 2θ, with interplanar distance, d and the miller indices (hkl) for sample A1 after heat treatment at 1100°C.

2θ	**d [Å]**	**h**	**k**	**l**
23.93	3.719	1	1	1
28.49	3.133	0	0	4
31.42	2.847	1	1	3
32.35	2.767	2	0	0
32.65	2.742	0	2	0
42.88	2.109	1	1	5
43.31	2.089	0	0	6
43.63	2.074	2	0	4
43.87	2.064	0	2	4
56.50	1.629	1	1	7
57.07	1.614	3	1	3
57.47	1.604	1	3	3
58.96	1.567	0	0	8

Table B.2: Lattice parameters for sample A1 at 1100°C

	A1 - 1100 °C
a [nm]	5.537
b [nm]	5.486
c [nm]	12.537

B.2 Sample B1 heat treated at 1100°C

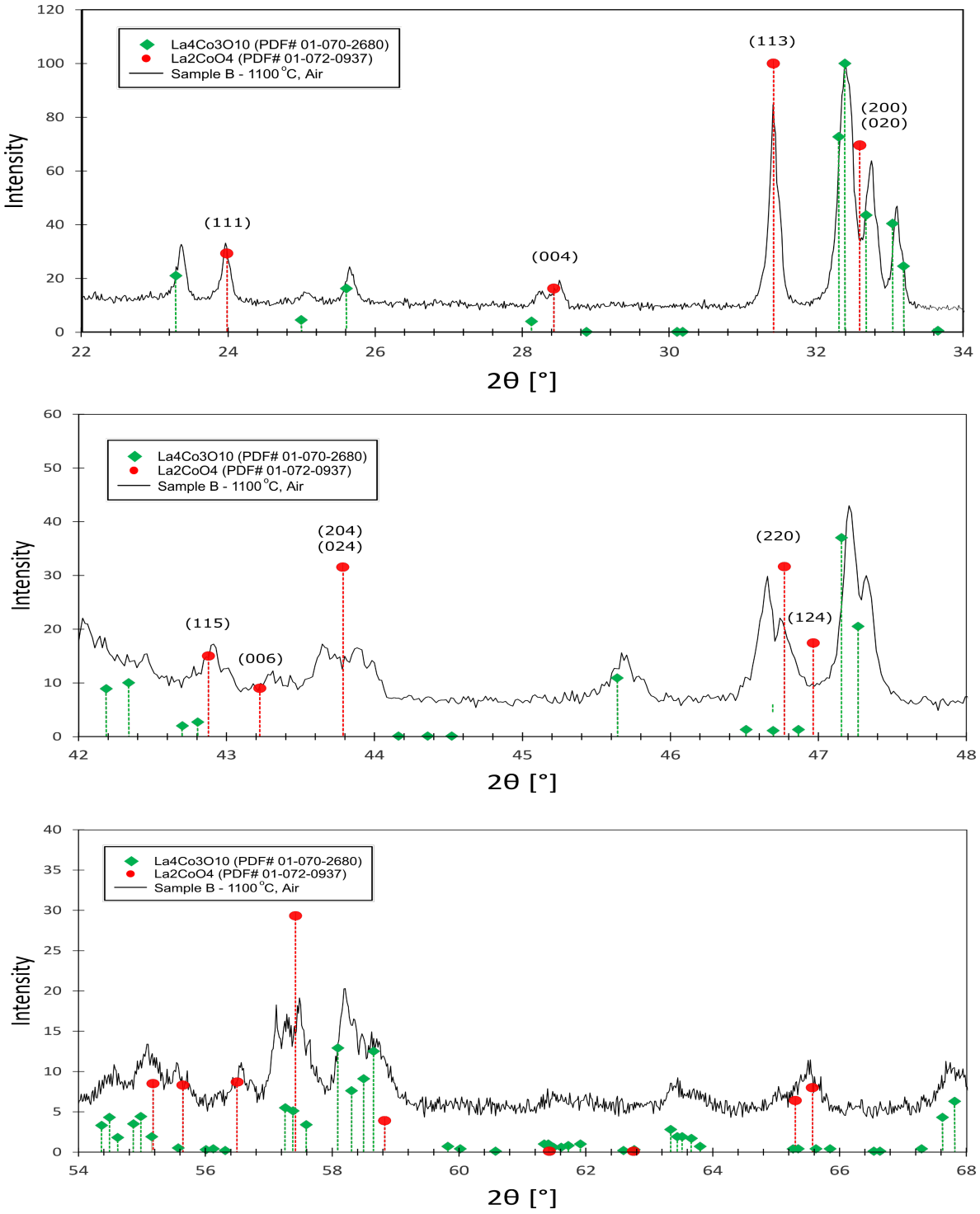

Figure B.2: Enlarged view of X-ray diffractogram of sample B1 in specific ranges; (top) $2\theta = 22 - 34°$ (middle) $2\theta = 42 - 48°$ (bottom) $2\theta = 54 - 68°$.

Table B.3: Position of peak related to the La_2CoO_4 phase, 2θ, with interplanar distance, d and the miller indices (hkl) for sample B1 after heat treatment at 1100°C.

2θ	**d [Å]**	**h**	**k**	**l**
23.98	3.711	1	1	1
28.52	3.129	0	0	4
31.42	2.847	1	1	3
42.91	2.107	1	1	5
43.33	2.088	0	0	6
43.68	2.072	2	0	4
43.92	2.062	0	2	4
56.53	1.628	1	1	7

Table B.4: Lattice parameters for sample B1 heat treated at 1100°C.

	B1 - 1100 °C
a [nm]	5.5250
b [nm]	5.4755
c [nm]	12.5383

B.3 Sample A1 after low-temperature oxidation

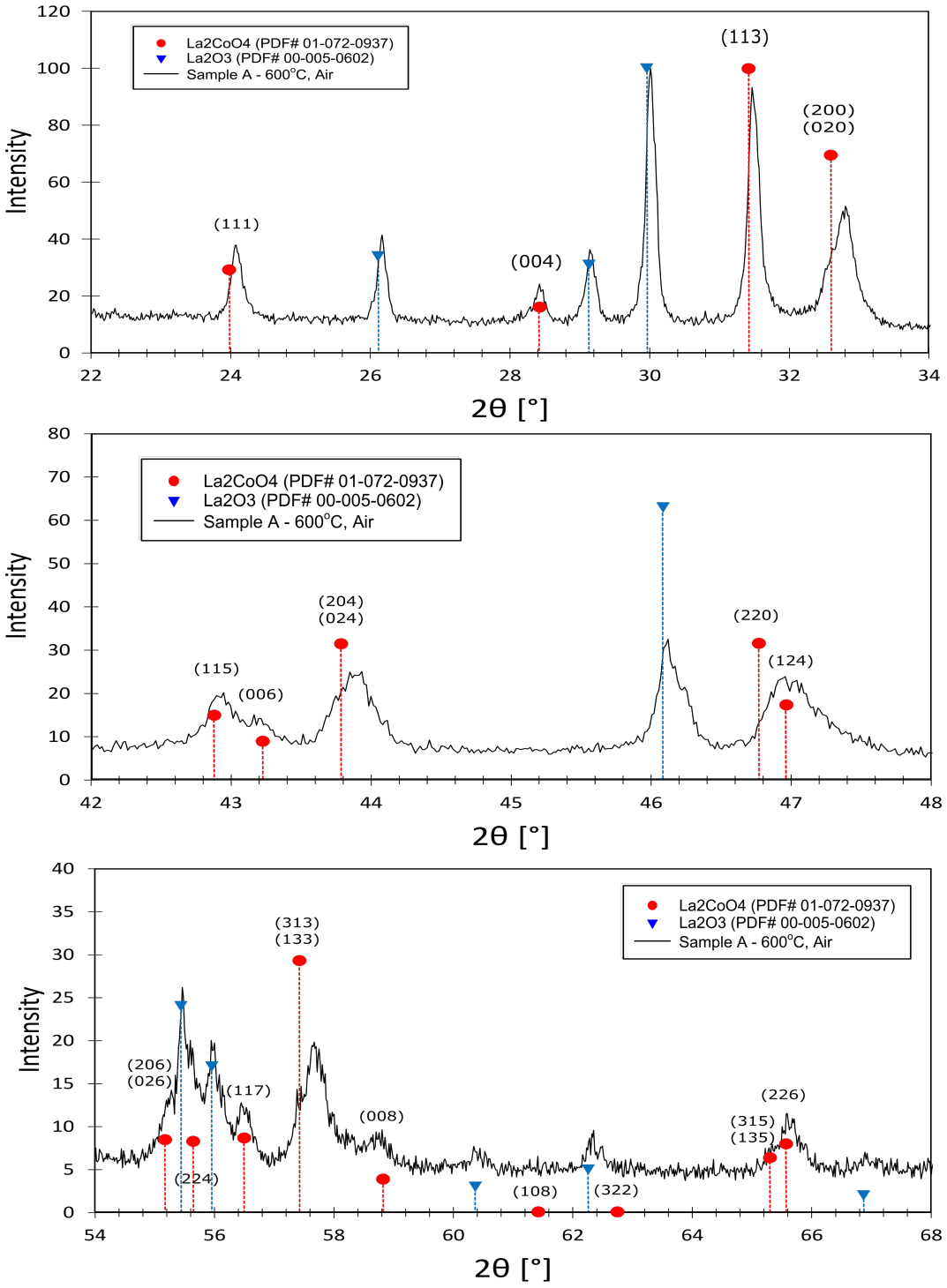

Figure B.3: Enlarged view of X-ray diffractogram of Sample A1 after low temperature oxidation in specific ranges; (top) $2\theta = 22-34°$ (middle) $2\theta = 42-48°$ (bottom) $2\theta = 54-68°$.

Table B.5: Position of peak related to the La_2CoO_4 phase, 2θ, with interplanar distance, d and the miller indices (hkl) for sample A1 after low-temperature oxidation.

2θ	**d [Å]**	**h**	**k**	**l**
24.08	3.696	1	1	1
28.47	3.135	0	0	4
31.47	2.843	1	1	3
42.95	2.106	1	1	5
43.85	2.065	0	0	6
56.53	1.628	1	1	7
58.86	1.569	0	0	8
65.59	1.423	2	2	6

Table B.6: Lattice parameters for sample A1 after low-temperature oxidation.

	A1 - 600 °C
a [nm]	5.5041
b [nm]	5.5041
c [nm]	12.5222

B.4 Sample B1 after low-temperature oxidation

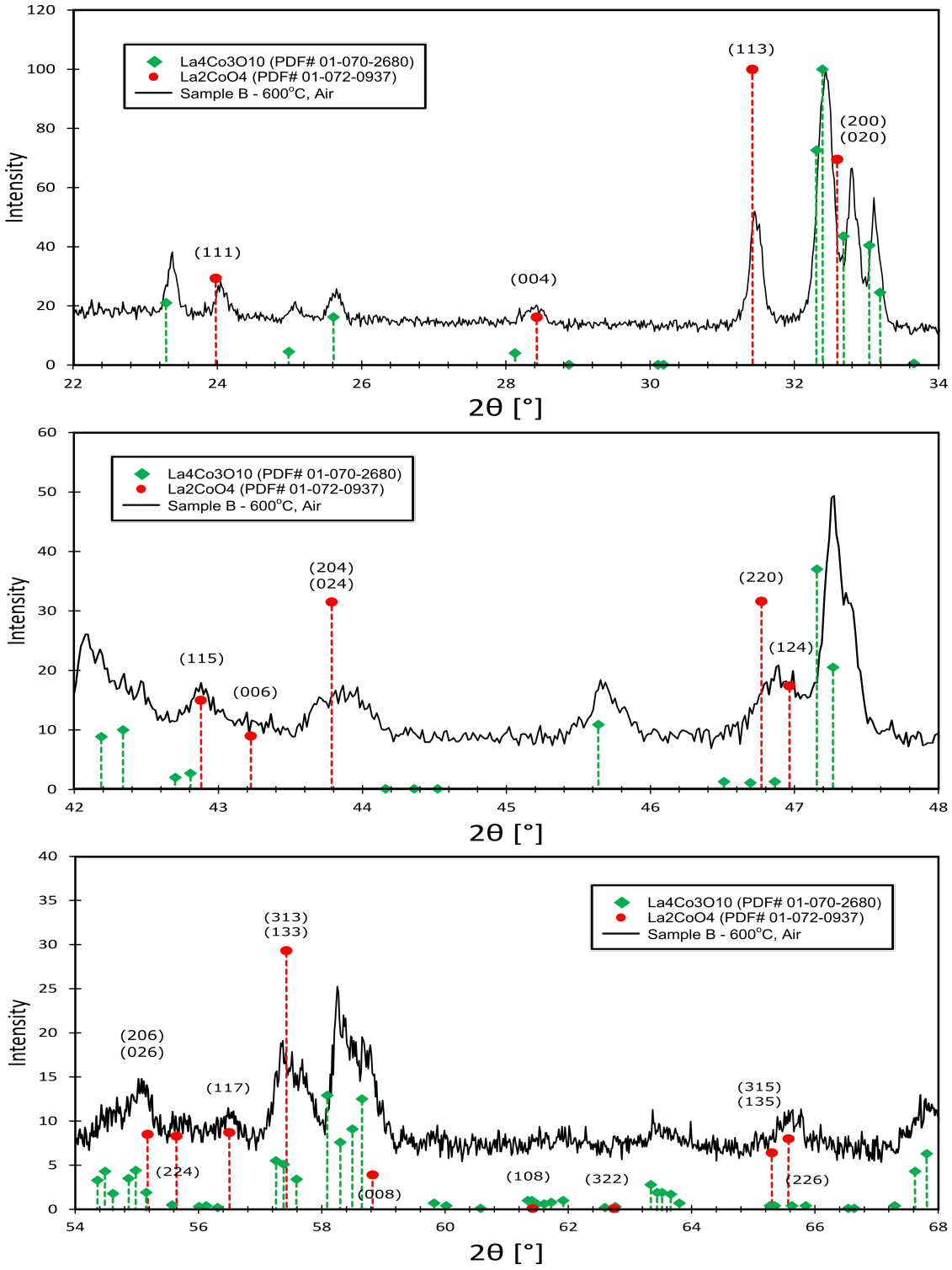

Figure B.4: Enlarged view of X-ray diffractogram of sample B1 after low-temperature oxidation; (top) $2\theta = 22 - 34°$ (middle) $2\theta = 42 - 48°$ (bottom) $2\theta = 54 - 68°$.

Table B.7: Position of peak related to the La_2CoO_4 phase, 2θ, with interplanar distance, d and the miller indices (hkl) for sample B1 after low-temperature oxidation.

2θ	**d [Å]**	**h**	**k**	**l**
24.06	3.698	1	1	1
28.44	3.138	0	0	4
31.47	2.843	1	1	3
42.88	2.109	1	1	5
46.99	1.934	1	2	4
56.53	1.628	1	1	7
43.71	2.071	2	0	4
43.87	2.064	0	2	4

Table B.8: Lattice parameters for sample B1 after low-temperature oxidation.

	B1 - 600 °C
a [nm]	5.479
b [nm]	5.479
c [nm]	12.559